Nucleation and stability of twins in hcp metals

L. Capolungo[1] and I. J. Beyerlein[2]
[1]*Materials Science and Technology Division, Los Alamos National Laboratory, Los Alamos, New Mexico 87545, USA*
[2]*Theoretical Division, Los Alamos National Laboratory, Los Alamos, New Mexico 87545, USA*
(Received 18 January 2008; revised manuscript received 1 April 2008; published 24 July 2008)

We propose a three-dimensional model for twin nucleation in hcp materials based on the nonplanar dissociation of the leading dislocation in a pile-up of $\langle a \rangle$ slip dislocations. Continuum linear elastic dislocation theory is used to calculate the change in free energy with extension of the dissociated configuration, consisting of a stair rod and glissile twinning dislocation loops. The model is applied to Mg, which deforms primarily by basal slip, and to Zr, which deforms primarily by prismatic slip. It is found that dissociations from an isolated $\langle a \rangle$ slip dislocation are energetically unable to produce a stable twin fault loop, at least larger than $2r_0$, the core width of the initial $\langle a \rangle$ slip dislocation. For some reactions, dissociations of the lead dislocation in a basal or prismatic dislocation pile-up can, however, lead to a stable and sizable twin loop. In these, the loop size is found to increase with decreasing twin boundary energy and increasing number of dislocations in the pile-up.

DOI: 10.1103/PhysRevB.78.024117 PACS number(s): 61.72.Mm, 61.72.Lk, 61.72.Nn, 61.72.Cc

I. INTRODUCTION

A. Deformation twinning

Twinning is a prevalent deformation mechanism in hexagonal-close-packed (hcp) metals. In contrast to face-centered cubic (fcc) metals, for which there is usually one twin mode, there are at least seven twinning modes (each with six variants) in hcp metals. Most of these twin types have been observed in one hcp metal or another under various deformation conditions.[1,2]

It has been suggested that twinning occurs by the nucleation and glide of twinning dislocations on their twin planes.[3,4] The concept of twinning dislocations was first graphically introduced in early work by Thompson and Millard.[5] Later, in works by Pond and Hirth[6] and by Serra *et al.*,[7] topological descriptions of a twinning dislocation, rigorously defined as an admissible interfacial defect belonging to the class of broken symmetry of which there are three, were developed. From these, a twinning dislocation can simply be thought of, at least for the purposes of this work, as a line defect having both a dislocation and step character. The height of the step character is dependent on the type of dislocation and consists of n crystallographic planes. When $n > 1$, the distortion caused by a single twinning dislocation is not restricted to a single plane, but affects n planes. In this case, the glide of a twinning dislocation will involve glide on each of the n planes along with some small corrective shuffling which places the atoms in their proper position.[7,8] The net Burgers vector of the ensemble is b_{twin}. Such a twinning dislocation is zonal.

When the twinning dislocation propagates on its glide plane, it creates a fault and reorients the lattice on one side of the fault to the mirror image of the other. Unlike slip, twinning dislocations can only shear material in one sense along b_{twin} and on their twin plane. Twin reorientation, Burgers vector, and glide plane depend on twin type and c/a ratio.

B. Previous twin nucleation models for hcp metals

The very few twin nucleation models for hcp metals presented to date can be classified, in our view, as either homogeneous or heterogeneous nucleation models. Homogeneous nucleation refers to a nucleation process that does not directly result from the presence of a defect (e.g., dislocation, grain boundary), and heterogeneous nucleation refers to one that does. Common features are the requirement of large stresses (or stress concentrations) in the vicinity of the nucleation event and an energy balance between the applied work, twin boundary energy, and strain energy produced by the twin shear. The first twin nucleation model belonged to the homogeneous class, and was introduced by Orowan[9] who considered twins to grow from a lenticular-shaped twin volume of uniform twin shear, multiple crystallographic layers thick. Based on this concept, Yoo and Lee[10,11] represented the twin nucleus as an inclusion in an isotropic medium using Eshelby's solution, which imparts an eigenstrain and a change in free energy of the system from that of a homogeneous system. Using a similar approach, Lebensohn and Tomé[12] studied the effect of the stress state on twin nucleation, showing that the contribution of hydrostatic pressure is negligible compared to that of the resolved shear stress. Because these homogeneous nucleation models require unreasonably high stresses,[1,2] heterogeneous nucleation models are also worth considering. For the first one in this class, Thompson and Millard[5] introduced a pole mechanism which results from the nonplanar dissociation of $\langle c \rangle$ dislocations into twinning dislocations. Later, in impressively much more detail, Mendelson derived several nonplanar dissociation reactions from $\langle a \rangle$, $\langle c+a \rangle$, or $\langle c \rangle$ dislocations leading to the generation of one or more glissile twinning dislocations on their respective twin planes.[3,13] Based on a study of $(\bar{2}111)$ twins in Co, Vaidya and Mahajan[14] proposed a combination reaction of $\langle a \rangle$ and $\langle c+a \rangle$ slip dislocations producing a 12-layer twin nucleus for this twin type.

C. Twin nucleation by dislocation dissociation

Mendelson[3,13] demonstrated that even with strict crystallographic requirements, the number of possible slip dislocation dissociations producing glissile twinning partials is still large ($\sim$80), varying with the originating slip dislocation

(e.g., basal, prismatic, or pyramidal), its Burgers vector, its character (screw, mixed, or edge), its strength (perfect versus partial), and with the type of twin plane.[13] In contrast, there are only ten possible dissociations from a slip dislocation in an fcc metal.[15]

Following a favorable dissociation event, the twinning dislocation(s) will assume an equilibrium distance d_s from the reaction center. The breaking of the core of a slip dislocation as well as stable extensions distances of $d_s \leq 2r_0$—where r_0 refers to the slip dislocation core radius—can only be treated by atomistic simulations. However, if $d_s > 2r_0$, then the energy and stability associated with the dissociation event can, in principle, be calculated using continuum dislocation theory. In this case, the larger d_s, the more likely the twinning dislocation can breakaway under a suitably oriented stress state, propagate across the grain, and trigger further events that lead to either formation of the twin nucleus or successive twin growth. Therefore, calculation of the energy and stable extension d_s of the configuration after the dissociation has occurred—including all product partial dislocations, not just the twinning dislocations—constitutes the critical next step in determining the favorability of twin nucleation by dissociation. For those few reactions described earlier[3,5,13,16,17] this has yet to be done.

For twins in cubic metals, on the other hand, dissociations of slip dislocations into stacking faults and eventually twin nuclei have been considered quite comprehensively using transmission electron microscopy (TEM), dislocation theory, density-functional theory, and molecular dynamics (MD).[17–20] For both bcc and fcc metals, the likely structure of the twin nucleus apparently consists of three adjacent planes of low energy stacking faults.[21–24] The structure of a twin nucleus in an hcp metal, however, has yet to be determined for a given twin type. Even without such information, it is conceivable that a sufficiently large glide extension $d_s > 2r_0$ of the first twinning dislocation could represent a critical step in forming the twin nucleus.

Elucidating the events leading to twin nucleus formation appears to be a well suited problem for atomistic models. To date, such molecular studies—using lj56, ti12, and na56 potentials[7,25] for ideal hcp structures or many-body potentials for α–Ti[26] and for Mg[27] and Zr[27]—have been successful in predicting approximate twin boundary structures and energies for certain metals and twin types. (In general, atomistic simulations and first-principle calculations[28] predict twin boundary energies within an order of magnitude.) In these, dissociations of slip dislocations at pre-existing twin boundaries have been simulated.[26,29] However, atomistic simulations are still limited by the availability of appropriate potentials for any given hcp metal. The proposed dissociations in Mendelson[3,13] for twinning dislocation production in hcp metals have yet to be tested. A representative simulation of this sort would need to include, not just the twinning partial of interest, but also the influence of the other partial dislocations produced by the dissociation.

D. Objectives

The present study investigates the mechanism of twin nucleation via nonplanar dissociations of $\langle a \rangle$ slip dislocations from either the basal or prismatic planes onto the seven possible twinning planes: $(\bar{2}111)$, $(\bar{2}112)$, $(\bar{2}113)$, $(\bar{2}114)$, $(\bar{1}011)$, $(\bar{1}012)$, $(\bar{1}013)$. The energy and stability of the extended core after the dissociation are calculated using continuum dislocation theory. The model is applied to magnesium (Mg) which deforms primarily by basal slip and zirconium (Zr) which deforms primarily by prismatic slip.

The model is three-dimensional (3D) and the twinning dislocations are loops, so that possible dependencies on dislocation length can manifest. Elastically favorable reactions are based on the ability of dissociated core to extend stably into a twin fault loop of a sufficient size, much larger than that of $a = |\langle a \rangle|$ or the core radius r_0 of the parent slip dislocation r_0. Due to lack of information concerning the embryonic structure of hcp twins, we will focus only on the production of the first stable twin fault loop per twin plane, rather than the construction of a twin nucleus. This stable twin loop, of size d_s, may be a precursor to a more complex twin nucleus structure or the twin nucleus itself.

The effects on d_s of dissociation type, initial dislocation length and character, twin boundary energy, and the stress τ (or activation energy) to cause the dissociation, are examined. In all cases studied, d_s after the dissociation of a single $\langle a \rangle$ slip dislocation is approximately $2r_0$ or less, suggesting that this set of reactions is not a viable mechanism for production of twinning dislocations. Significantly it is shown that this result is independent of τ. For some dissociations, a sufficiently large loop ($10r_0$ or larger) can be produced if the dissociation occurs at the head of a relatively small pile-up of slip dislocations (5 to 10). In these cases, the pile-up supplies a repulsive force that repels the twinning dislocation away from the core center and extends the stable twin fault. The ability for a pile-up to do so depends on the configuration and character of all the dissociation products, and consequently a pile-up will not alter the stable fault loop size for every dissociation, as will be demonstrated.

II. DEFORMATION TWINNING IN HCP METALS

A. Twinning partial dislocations

The seven twin planes in hcp metals, $(\bar{2}111)$, $(\bar{2}112)$, $(\bar{2}113)$, $(\bar{2}114)$, $(\bar{1}011)$, $(\bar{1}012)$, $(\bar{1}013)$, are illustrated in Fig. 1. The corresponding shear directions are: $1/3[\bar{2}11\bar{6}]$, $1/3[\bar{2}113]$, $[\bar{2}112]$, $[\bar{1}012]$, $[\bar{1}011]$, $[\bar{3}032]$, respectively.

As mentioned in Sec. I, some types of twinning dislocations may distort more than one lattice plane, in which case they are classified as zonal dislocations.[5,8,13] In what follows, n denotes the number of planes on which the twinning dislocation lies. Clearly, n can be known solely with molecular simulations. In the following analytical treatment, the same methodology as that introduced by Mendelson will be adopted. Specifically, for a given twin type, the twin shear S can be known from simple geometrical considerations. If d_{twin} denotes the distance between two consecutive twin planes and b_{twin} denotes the norm of the Burgers vector of the twinning dislocation, then S must be:

$$S = \frac{b_{\text{twin}}}{n d_{\text{twin}}}. \tag{1}$$

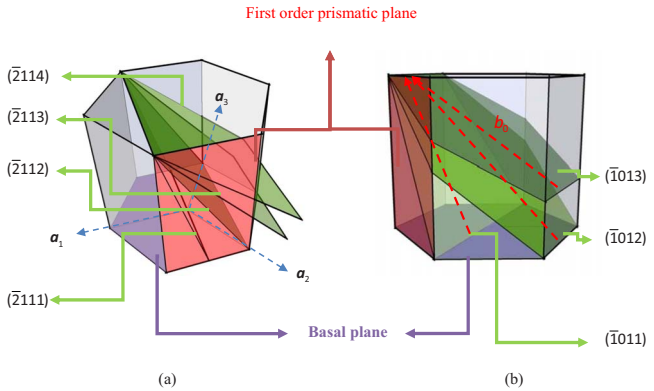

FIG. 1. (Color online) Schematic of the (a) $(\bar{2}11X)$ twin modes and (b) $(\bar{1}01X)$ twin modes.

b_{twin} can be related to a proportionality coefficient s and b_0, the norm of a reference vector $\langle b_0 \rangle$ parallel to the twinning dislocation, by:

$$b_{\text{twin}} = sb_0, \tag{2}$$

where $\langle b_0 \rangle$ is given by:

$$\langle b_0 \rangle = \rho\langle a \rangle + \frac{\sigma}{2}\langle c \rangle \quad \text{for } (\bar{2}11X) \text{ planes with } X = 1, \ldots, 4$$

$$\langle b_0 \rangle = \rho\langle d \rangle + \frac{\sigma}{2}\langle c \rangle \quad \text{for } (\bar{1}01X) \text{ planes with } X = 1, \ldots, 3. \tag{3}$$

Here $\langle a \rangle = 1/3\langle \bar{2}110 \rangle, \langle c \rangle = \langle 0001 \rangle$ and $\langle d \rangle = 1/3\langle \bar{1}010 \rangle$. Values of ρ and σ corresponding to each twinning plane are given in Table I. Let s' denote the necessary shear to create a one of the fault layers of n. From geometrical considerations, Mendelson[3,13] related n and s' to s through:

$$s = ns' - p, \tag{4}$$

where p is chosen such that the absolute value of s is smaller than 1. s' is given by:

$$s' = \frac{1}{\left[\rho + \left(\frac{\sigma^2}{4\rho}\right)\left(\frac{c}{a}\right)^2\right]} \quad \text{for } (\bar{2}11X) \text{ planes with } X = 1, \ldots, 4$$

and

TABLE I. Parameters defining the elementary shear for each twinning dislocation.

	$(\bar{2}111)$	$(\bar{2}112)$	$(\bar{2}113)$	$(\bar{2}114)$	$(\bar{1}011)$	$(\bar{1}012)$	$(\bar{1}013)$
ρ	1	1	3	2	3	3	9
σ	4	2	4	2	4	2	4

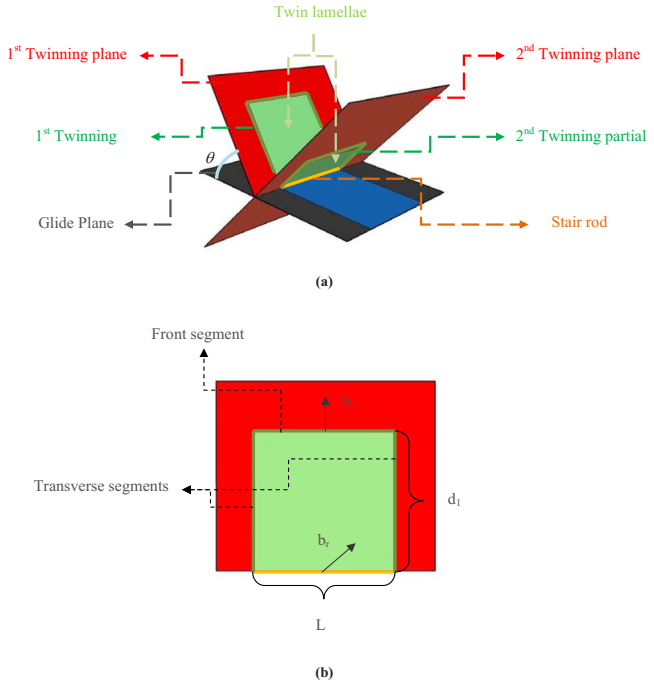

FIG. 2. (Color online) Schematic of the (a) dissociation of a slip dislocation into twinning dislocations, and (b) first partial dislocation loop on the first twinning plane.

$$s' = \frac{1}{\left[\frac{\rho}{3} + \left(\frac{\sigma^2}{4\rho}\right)\left(\frac{c}{a}\right)^2\right]} \quad \text{for } (\bar{1}01X) \text{ planes with } X = 1, \ldots, 3. \tag{5}$$

With Eqs. (1)–(5), n is chosen such that the absolute value of s is the smallest. Depending on the sign of s, the twinning partial will propagate in its twin plane either above (as shown in Fig. 2(a) for $s > 0$) or below the slip plane of the originating dislocation. With this criterion, twinning directionality is enforced.

B. Dislocation dissociations

Mendelson[3] determined the possible ways a (stationary) slip dislocation can dissociate to produce one or more glissile twinning dislocation(s). With very few exceptions, the dissociated configurations are nonplanar and consist of a twinning dislocation (or dislocations) and a stair rod lying between the slip plane of the original dislocation and twin plane(s). These dissociations obey two rules: (1) the locus of the dislocation line must coincide with the line of intersection of the slip plane and twinning plane, and (2) the Burgers vector of the twinning dislocations must engender the necessary shear for twinning. The first means that the slip dislocation must have the appropriate character and orientation, suggesting that twin nucleation will be probabilistic in nature. The second means that at least one of the reaction products is a twinning dislocation that lies on its twinning plane.

From these dissociations, one or more twinning dislocations may be produced. When two or more are produced, they either will be two different variants of the same twin

type, or will belong to different twin types. The first case is called a symmetric dissociation because the like-twinning dislocations will extend symmetrically from the stair rod under a uniform stress state. (In the presence of a nonuniform stress field, from say, nearby dislocations, locked obstacles, walls, grain boundaries, pile-ups, however, they will not.) The second case leads to an asymmetric dissociation, because the twin boundary energy, twin shear, Burgers vector, and twin plane orientation differ between the twinning dislocations.

The present formulation considers a 3D representation, in which twinning dislocations propagate as loops. A 3D schematic of an asymmetric, double dissociation is presented in Fig. 2(a). A twin loop will be approximated as a rectangle, as detailed in Fig. 2(b), with two transverse segments of length d and front segment of length L. It is assumed that this loop expands from the stair rod by propagation in d, while L remains constant. The Burgers vector of the stair rod dislocation is denoted b_r and can either be pure edge or mixed. The Burgers vectors of the first and second twinning loops are b_{t1} and b_{t2}, wherein each segment will either be pure edge or screw.

Numerous dissociation reactions respect Mendelson's two conditions; however, in this work, we will consider only dissociations from slip dislocations with Burgers vector $\langle a \rangle = 1/3\langle \bar{2}110 \rangle$, from either the basal plane (Tables II and III) or the prismatic plane (Table IV). As shown, the number of such dissociations is still large and covers a wide range of hcp metals from Be, Zn, Cd, and Mg, which deform primarily by basal slip, and Ti and Zr, which deform primarily by prismatic slip. Single and double dissociations of a perfect $\langle a \rangle$ basal dislocation are presented in Table II, single and double dissociations of a Shockley partial dislocation from the basal plane onto the $(\bar{1}01X)$ planes $(X=1, \ldots,3)$ in Table III, and single dissociations of a perfect prismatic $\langle a \rangle$ dislocation in Table IV. Double dissociations involve twinning dislocations of the same type. To classify each dissociation in Tables II–IV, the following notations are used: α refers to either a single $(\alpha=1)$ or a double $(\alpha=2)$ dissociation; the initial configuration (*Init.*) refers to the glide plane (*Bas.* for basal and *Prism.* for prismatic); *Perf.* means perfect slip dislocations and *Part.* means partial slip dislocations; the character of the stair rod dislocation segment is presented in column "*Stair Rod*" where *E*, *S*, or *M* refers to edge, screw, or mixed character; and the character of the twinning dislocation (including n and the edge/screw character of each segment in the loop) is presented in column *Twin. Dis.*

Also provided is the dissociation reaction, where the left-hand side corresponds to the Burgers vector of the initial slip dislocation, and the right-hand side lists from left to right, b_r, b_{t1}, and b_{t2}. In these, recall that $\langle a \rangle$, $\langle c \rangle$, and $\langle d \rangle$ refer to Burgers vectors $1/3\langle \bar{2}110 \rangle$, $\langle 0001 \rangle$, and $1/3\langle \bar{1}010 \rangle$, respectively.

The utility of these tables is best understood by taking a specific example. Consider the dissociation in the last line of Table II:

$$\langle a \rangle \rightarrow [(\langle a \rangle - 9s\langle d \rangle - 2s\langle c \rangle) + s(9\langle d \rangle + 2\langle c \rangle)]. \quad (6)$$

As shown in Table II, Eq. (6) corresponds to a perfect basal dislocation with Burgers vector $\boldsymbol{b}_{\text{ini}} = \langle a \rangle = 1/3\langle \bar{2}110 \rangle$ that dissociates into a stair rod dislocation of mixed character and a twinning dislocation with an edge front segment and screw transverse segments. The twinning dislocation lies on the $(\bar{1}013)$ plane with Burgers vector: $\boldsymbol{b}_{t1} = s(9\langle d \rangle + 2\langle c \rangle)$. The Burgers vector of the stair rod is $\boldsymbol{b}_r = \langle a \rangle - 9s\langle d \rangle - 2s\langle c \rangle$. From Table I, $\rho=9$ and $\sigma=4$ for the $(\bar{1}013)$ plane and with Eq. (5), s' can be calculated. With $n=4$, as indicated in Table II, s can finally be calculated with Eq. (4).

For dissociations of perfect basal dislocations, presented in Table II, the front segment is pure edge, while the transverse segments are pure screw. All dissociations onto the $\langle 01\bar{1}0 \rangle$ zone axis yield pure edge stair rod dislocations, while dissociations onto the $\langle 1\bar{2}10 \rangle$ zone axis yield mixed stair rod dislocations, a difference which could alter the stable configurations between these two classes of twins. b_r also will differ in the case of $\alpha=1$ and $\alpha=2$; for $\alpha=1$, b_r remains on the glide plane, while for $\alpha=2$, it reorients to a different plane. The reorientation could act as a locking mechanism, possibly anchoring the stair rod dislocation as the twinning dislocations glide away.

Also of interest are dissociations of an extended basal dislocation (Table III). Particularly when the basal stacking fault energy is low, basal dislocations will find it energetically favorable to split apart in their glide plane into two Shockley partials separated by a stacking fault by the following reaction:

$$\langle a \rangle \rightarrow \langle d \rangle + \langle d' \rangle, \quad (7)$$

where $\langle d' \rangle = 1/3\langle \bar{1}100 \rangle$. Nonplanar dissociations into twinning dislocations of the lead Shockley partial $\langle d \rangle$ are presented in Table III. Simple geometric considerations explains why these dissociations can lead to twinning dislocations onto the $(\bar{1}01X)$ planes $(X=1, \ldots,3)$, but not the $(\bar{2}11X)$ planes $(X=1, \ldots,4)$. Following the dissociation of the lead, the trailing partial remains on the glide plane and assumes an equilibrium distance d'_{eq} with the stair rod dislocation.

In the case of dissociations of prismatic dislocations, presented in Table IV, the front segments of the twinning dislocations are pure screw, contrary to the reactions presented previously. Accordingly, the two transverse segments are pure edge and their interaction is repulsive. From this, one can appreciate that L [Fig. 2(b)] may affect the energetics of such dissociations more so than for basal dislocation reactions in Tables II and III. Moreover, the angle between a prismatic plane and any of the $(\bar{2}11X)$ twin planes is fixed at 90°, while the angle between a prismatic plane and the $(\bar{1}01X)$ twin planes depends on the c/a ratio and particular value of $X=1, \ldots,3$, of the $(\bar{1}01X)$ plane. This difference will also have important energetic consequences, as will be seen later.

C. Energetic considerations

1. Formation of a stable twin fault loop

In the present model the size of the stable *twin nucleus*, d_s is defined as the stable dissociation extension d of the transverse twinning dislocation. A schematic of the total energy E

TABLE II. Dissociations of perfect basal slip dislocations, where M (Mixed), S (Screw), E (Edge), and $\langle a\rangle = 1/3\langle\bar{2}110\rangle$, $\langle c\rangle = \langle 0001\rangle$, $\langle d\rangle = 1/3\langle\bar{1}010\rangle$.

α	Init.	Twin. Plane	Reaction: $\langle b_{\mathrm{ini}}\rangle \rightarrow \langle b_r\rangle + \langle b_{t1}\rangle + \langle b_{t2}\rangle$	Stair Rod	Twin. Dis. # planes	Twin. Dis. Ft. Seg.	Twin. Dis. Tr. Seg.
2	Bas. Perf.	$(\bar{2}111)$	$\langle a\rangle \rightarrow \begin{bmatrix}(1-2s)\langle a\rangle + s(\langle a\rangle + 2\langle c\rangle) \\ + s(\langle a\rangle - 2\langle c\rangle)\end{bmatrix}$	E	1	E	S
2	Bas. Perf.	$(\bar{2}112)$	$\langle a\rangle \rightarrow \begin{bmatrix}(1-2s)\langle a\rangle + s(\langle a\rangle + \langle c\rangle) \\ + s(\langle a\rangle - \langle c\rangle)\end{bmatrix}$	E	1–3	E	S
2	Bas. Perf.	$(\bar{2}113)$	$\langle a\rangle \rightarrow \begin{bmatrix}(1-6s)\langle a\rangle + s(3\langle a\rangle + 2\langle c\rangle) \\ + s(3\langle a\rangle - 2\langle c\rangle)\end{bmatrix}$	E	1	E	S
2	Bas. Perf.	$(\bar{2}114)$	$\langle a\rangle \rightarrow \begin{bmatrix}(1-4s)\langle a\rangle + s(2\langle a\rangle + \langle c\rangle) \\ + s(2\langle a\rangle - \langle c\rangle)\end{bmatrix}$	E	3–4	E	S
2	Bas. Perf.	$(\bar{1}011)$	$\langle a\rangle \rightarrow \begin{bmatrix}(\langle a\rangle - 6s\langle d\rangle) + s(3\langle d\rangle + 2\langle c\rangle) \\ + s(3\langle d\rangle - 2\langle c\rangle)\end{bmatrix}$	M	4	E	S
2	Bas. Perf.	$(\bar{1}012)$	$\langle a\rangle \rightarrow \begin{bmatrix}(\langle a\rangle - 6s\langle d\rangle) + s(3\langle d\rangle + \langle c\rangle) \\ + s(3\langle d\rangle - \langle c\rangle)\end{bmatrix}$	M	2	E	S
2	Bas. Perf.	$(\bar{1}013)$	$\langle a\rangle \rightarrow \begin{bmatrix}(\langle a\rangle - 18s\langle d\rangle) + s(9\langle d\rangle + \langle c\rangle) \\ + s(9\langle d\rangle - \langle c\rangle)\end{bmatrix}$	M	4	E	S
1	Bas. Perf.	$(\bar{2}111)$	$\langle a\rangle \rightarrow [((1-s)\langle a\rangle - 2s\langle c\rangle) + s(\langle a\rangle + 2\langle c\rangle)]$	E	1	E	S
1	Bas. Perf.	$(\bar{2}112)$	$\langle a\rangle \rightarrow [((1-s)\langle a\rangle - s\langle c\rangle) + s(\langle a\rangle + \langle c\rangle)]$	E	1–3	E	S
1	Bas. Perf.	$(\bar{2}113)$	$\langle a\rangle \rightarrow [((1-3s)\langle a\rangle - 2s\langle c\rangle) + s(3\langle a\rangle + 2\langle c\rangle)]$	E	1	E	S
1	Bas. Perf.	$(\bar{2}114)$	$\langle a\rangle \rightarrow [((1-2s)\langle a\rangle - s\langle c\rangle) + s(2\langle a\rangle + \langle c\rangle)]$	E	3–4	E	S
1	Bas. Perf.	$(\bar{1}011)$	$\langle a\rangle \rightarrow [(\langle a\rangle - 3s\langle d\rangle - 2s\langle c\rangle) + s(3\langle d\rangle + 2\langle c\rangle)]$	M	4	E	S
1	Bas. Perf.	$(\bar{1}012)$	$\langle a\rangle \rightarrow [(\langle a\rangle - 3s\langle d\rangle - s\langle c\rangle) + s(3\langle d\rangle + \langle c\rangle)]$	M	2	E	S
1	Bas. Perf.	$(\bar{1}013)$	$\langle a\rangle \rightarrow [(\langle a\rangle - 9s\langle d\rangle - 2s\langle c\rangle) + s(9\langle d\rangle + 2\langle c\rangle)]$	M	4	E	S

TABLE III. Dissociations of partial basal slip dislocations, where $\langle a\rangle = 1/3\langle\bar{2}110\rangle$, $\langle c\rangle = \langle 0001\rangle$, $\langle d\rangle = 1/3\langle\bar{1}010\rangle$.

α	Init.	Twin. Plane	Reaction: $\langle b_{\text{ini}}\rangle \rightarrow \langle b_r\rangle + \langle b_{t1}\rangle + \langle b_{t2}\rangle$	Stair Rod	Twin. Dis. # planes	Twin. Dis. Ft. Seg.	Twin. Dis. Tr. Seg.
2	Bas. Part.	$(\bar{1}011)$	$\langle d\rangle \rightarrow \begin{bmatrix} (\langle d\rangle - 6s\langle d\rangle) + s(3\langle d\rangle + 2\langle c\rangle) \\ + s(3\langle d\rangle - 2\langle c\rangle) \end{bmatrix}$	E	4	E	S
2	Bas. Part.	$(\bar{1}012)$	$\langle d\rangle \rightarrow \begin{bmatrix} (\langle d\rangle - 6s\langle d\rangle) + s(3\langle d\rangle + \langle c\rangle) \\ + s(3\langle d\rangle - \langle c\rangle) \end{bmatrix}$	E	2	E	S
2	Bas. Part.	$(\bar{1}013)$	$\langle d\rangle \rightarrow \begin{bmatrix} (\langle d\rangle - 18s\langle d\rangle) + s(9\langle d\rangle + \langle c\rangle) \\ + s(9\langle d\rangle - \langle c\rangle) \end{bmatrix}$	E	4	E	S
1	Bas. Part.	$(\bar{1}011)$	$\langle d\rangle \rightarrow [(\langle d\rangle - 3s\langle d\rangle - 2s\langle c\rangle) + s(3\langle d\rangle + 2\langle c\rangle)]$	E	4	E	S
1	Bas. Part.	$(\bar{1}012)$	$\langle d\rangle \rightarrow [(\langle d\rangle - 3s\langle d\rangle - s\langle c\rangle) + s(3\langle d\rangle + \langle c\rangle)]$	E	2	E	S
1	Bas. Part.	$(\bar{1}013)$	$\langle d\rangle \rightarrow [(\langle d\rangle - 9s\langle d\rangle - 2s\langle c\rangle) + s(9\langle d\rangle + 2\langle c\rangle)]$	E	4	E	S

versus d profile for an energetically feasible dissociation leading to d_s is shown in Fig. 3. The initial value E_{ini} is, in this example, the self-energy of the isolated slip dislocation. Given a sufficient amount of energy (or stress) E_{activ}, its core dissociates and separates until an unstable extension d_c is reached after which the partials can freely expand to a stable separation d_s. The maximum energy configuration at d_c is E_{nucl} and the free activation energy E_{activ} is the difference between E_{ini} and E_{nucl}. A stable configuration is reached at separation d_s when E is at a saddle point, mathematically defined as:

$$\frac{\partial E}{\partial d} = 0, \quad \frac{\partial^2 E}{\partial d^2} \geq 0, \quad d = d_s. \tag{8}$$

There are two consecutive steps in twin nucleation mentioned here, dissociation and extension, where the transition point roughly occurs at $d = 2r_0$. In the first step, the activation energy or stress required to cause the split, as well as changes in core energies before and after the split, are best accessed through atomistic calculations. Only the second step is theoretically treated in this work and the energy and stability of the product partials after the dissociation are calculated. After the dissociation, the contributions to E are calculated using linear elastic dislocation theory, which is valid for distances $2r_0$ beyond the core of the dislocations. Below $2r_0$, Hooke's law does not apply and the cores of the slip dislocation, stair rod, and twinning dislocations are not yet distinguishable. If, however, $d_s > 2r_0$, we consider the disso-

TABLE IV. Dissociations of perfect prismatic slip dislocations, where $\langle a\rangle = 1/3\langle\bar{2}110\rangle$, $\langle c\rangle = \langle 0001\rangle$, $\langle d\rangle = 1/3\langle\bar{1}010\rangle$.

α	Init.	Twin.Plane	Reaction: $\langle b_{ini}\rangle \rightarrow \langle b_r\rangle + \langle b_{t1}\rangle + \langle b_{t2}\rangle$	Stair Rod	Twin. Dis. # planes	Twin. Dis. Ft. Seg.	Twin. Dis. Tr. Seg.
1	Prism Perf.	$(\bar{2}111)$	$\langle a\rangle \rightarrow [((1-s)\langle a\rangle - 2s\langle c\rangle) + s(\langle a\rangle + 2\langle c\rangle)]$	M	1	S	E
1	Prism Perf.	$(\bar{2}112)$	$\langle a\rangle \rightarrow [((1-s)\langle a\rangle - s\langle c\rangle) + s(\langle a\rangle + \langle c\rangle)]$	M	1–3	S	E
1	Prism Perf.	$(\bar{2}113)$	$\langle a\rangle \rightarrow [((1-3s)\langle a\rangle - 2s\langle c\rangle) + s(3\langle a\rangle + 2\langle c\rangle)]$	M	1	S	E
1	Prism Perf.	$(\bar{2}114)$	$\langle a\rangle \rightarrow [((1-2s)\langle a\rangle - s\langle c\rangle) + s(2\langle a\rangle + \langle c\rangle)]$	M	3–4	S	E
1	Prism Perf.	$(\bar{1}011)$	$\langle a\rangle \rightarrow [(\langle a\rangle - 3s\langle d\rangle - 2s\langle c\rangle) + s(3\langle d\rangle + 2\langle c\rangle)]$	M	4	S	E
1	Prism Perf.	$(\bar{1}012)$	$\langle a\rangle \rightarrow [(\langle a\rangle - 3s\langle d\rangle - s\langle c\rangle) + s(3\langle d\rangle + \langle c\rangle)]$	M	2	S	E
1	Prims Perf.	$(\bar{1}013)$	$\langle a\rangle \rightarrow [(\langle a\rangle - 9s\langle d\rangle - 2s\langle c\rangle) + s(9\langle d\rangle + 2\langle c\rangle)]$	M	4	S	E

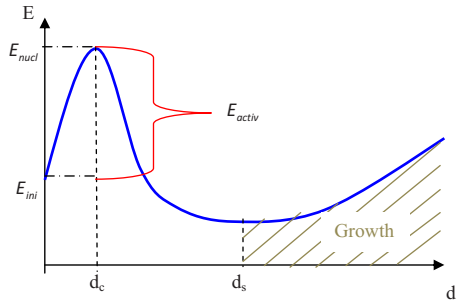

FIG. 3. (Color online) Schematic of the energy evolution of the system during a dissociation that produces a stable twin nucleus of size d_s.

ciation to have successfully created twinning dislocation(s) and faulted area(s), $d_s \times L$. In this event, the larger d_s, the more elastically favorable is the dissociation. The fate of the twin fault loop d_s, once formed, is beyond the scope of this work, but will be addressed later in the discussion.

Mendelson realized that the interaction forces between the twinning dislocation(s) and the stair rod must collectively be repulsive for the dissociation to be elastically favorable. For this, he applied continuum linear elastic dislocation theory to a two–dimensional (2D) representation of the dissociation. The sum of the interaction energies between all dislocations in the dissociated configuration with extension a was called γ_m (Ref. 3) and the dissociation was considered favorable when $\gamma_m > \gamma$, where γ is the twin boundary energy. However, a is too close to the inelastic core for the theory to be valid and provide meaningful insight on stability. Moreover, the 2D model overlooks several dislocation possible interactions, which we show using the 3D model in Fig. 2 to be important.

2. Energy contributions after dissociation

Calculations of E, therefore, begin at $d=2r_0$. We select $2r_0$ as an extreme limiting value, but d in the range of $2r_0$–$4r_0$ may still represent an unfavorable size for a twin fault loop, as one must account for errors in estimating r_0.

Following Nabarro,[30] E is the sum of the self-energies of the dislocations, the interaction energies between the dislocations, and the interaction energy between the applied forces and dislocations. After the splitting event, $d > 2r_0$, E is given by:

$$E = E_{t1} + 2E_{l1} + E_r + E_{r/t1} + E_{\text{prim}} - W + (\alpha - 1)(E_{t2} + 2E_{l2} + E_{t1/t2} + E_{r/t2}), \tag{9}$$

with $\alpha=1$ in the case of a single dissociation, $\alpha=2$ in the case of a double, and subscripts 1 and 2 refer to the first and second twinning dislocations. W is the work done by the twinning dislocation(s) in expansion under a given stress state τ and is:

$$W = L[\tau_{t1} \cdot b_{t1} \cdot d_1 + (\alpha - 1) \cdot \tau_{t2} \cdot b_{t2} \cdot d_2], \tag{10}$$

where τ_{t1} and τ_{t2} are the resolved shear stresses on the first and second twinning dislocations from τ and d_1 and d_2 are their corresponding extensions. In the calculations, we assume that the dissociation was activated by stress and considered a wide range of values for τ_{t1} and τ_{t2}: 0, 320, 640, and 1280 MPa, with 0 MPa corresponding to a spontaneous dissociation. Including W in E assumes that the shear stress is not removed after the dissociation and remains constant over the reaction region.

E_{t1}, E_{l1},E_r,$E_{r/t1}$, and $E_{t1/t2}$, denote the twin loop energy (to be defined later), the twin fault energy, the self-energy of the stair rod dislocation, the interaction energy between the stair rod dislocation and twinning dislocation, and the interaction energy between the two twinning dislocations. E_{prim} is the energy of those dislocations remaining on the primary glide plane after the dissociation apart from the stair rod.

Due to the 3D representation, it is necessary to calculate these energy contributions to recall some important results in dislocation theory regarding the separation of edge and screw segments in anisotropic media. Extending Eshelby's early result,[31] Foreman[32] showed that the most general elastic stiffness tensor that allows for the decomposition of the energy of a mixed dislocation into the sum of its screw and edge components has the following null components: c_{14}, c_{15}, c_{24}, c_{25}, c_{46}, c_{56}, when written in a local coordinate system with the dislocation line aligned with axis $3(z)$ and the plane normal aligned with axis $2(y)$. When their dislocation lines are nonparallel, such as the transverse and front segments of a twinning loop [Fig. 2(b)], their interaction energy was derived by Orlov and Indenbom[33] who extended Kroupa's formula[34,35] via a Green's function approach. Our interpretation of their result is that the interaction energy between edge and screw segments which lie normal to one another is null when the elastic tensor, written in the appropriate local coordinate system, has the same zero components as in an isotropic medium, i.e., c_{14}, c_{15}, c_{16}, c_{24}, c_{25}, c_{26}, c_{34}, c_{35}, c_{36}, c_{45}, c_{46}, c_{56}, regardless of the number of independent components.

The elastic tensor in the basal plane for most hcp metals, including the two metals Mg and Zr of interest here, respects the first condition (axis 2 is parallel to the c axis). Transformation of the elastic tensor for both Mg and Zr to the coordinate system of each glide plane and twin plane and for every dissociation in Tables II–IV finds that the components c_{14}, c_{15}, c_{16}, c_{24}, c_{25}, c_{26}, c_{34}, c_{35}, c_{36}, c_{45}, c_{46}, c_{56}, and their symmetric, are either zero or negligible. Therefore, the interactions between parallel and nonparallel edge and screw segments can be neglected in the following calculations.

We will normalize E by E_{ini}, the initial system energy. In the case of a dissociation from an isolated perfect dislocation (Tables II and IV), E_{ini} is its self-energy:[8]

$$E_{\text{ini}} = \frac{L}{4\pi}[K^e_{\text{ini}}(b^e_{\text{ini}})^2 + K^s_{\text{ini}}(b^s_{\text{ini}})^2]\ln\frac{R}{r_0}, \tag{11}$$

where b^e_{ini} and b^s_{ini} denote the edge and screw component of its Burgers vector. R and r_0 denote the outer and inner cutoff radii. K^e_{ini} and K^s_{ini} for the edge and screw parts depend on the elastic constants (written in the appropriate coordinate system defined by the glide plane and glide direction of the dislocation) and Burgers vectors.[36] The procedure used here to calculate K^e_{ini} and K^s_{ini} can be found in Hirth and Lothe.[8] In

the case of an extended dislocation (Table III), E_{ini} is given by:

$$E_{\text{ini}} = \frac{L}{4\pi}[K^e_{\text{ini1}}(b^e_{\text{ini1}})^2 + K^s_{\text{ini1}}(b^s_{\text{ini1}})^2 + K^e_{\text{ini2}}(b^e_{\text{ini2}})^2 + K^s_{\text{ini2}}(b^s_{\text{ini2}})^2]\ln\frac{R}{r_0} + \Gamma^{SF}\cdot L\cdot d^{eq}_{\text{ini}}, \tag{12}$$

where subscripts ini1 and ini2 refer to the first and second partial dislocation. Γ^{SF} and d^{eq}_{ini} denote the stacking fault energy and the equilibrium distance between the partial dislocations, which is simply:

$$d^{eq}_{\text{ini}} = K^e_{\text{ini1}}\frac{b^e_{\text{ini1}}\cdot b^e_{\text{ini2}}}{2\pi\cdot\Gamma^{SF}} \tag{13}$$

because the leading partial is pure edge (as indicated in Table III). When the dislocation that dissociates is at the head of an N-sized pile-up, E_{ini} is:[8]

$$E_{\text{ini}} \approx \frac{K^e_{\text{ini}}(b^e_{\text{ini}})^2N^2}{4\pi}\ln\frac{4R}{l} + \frac{K^s_{\text{ini}}(b^s_{\text{ini}})^2N^2}{4\pi}\ln\frac{4R}{l}, \tag{14}$$

with $R \gg l$, the length of the dislocation pile-up. For our purposes, the simple approximation, $l=Nr_0$ is sufficient, but keeping in mind that generally l is inversely proportional to τ. Precise values would be required when say estimates of the back stress or stress field ahead of the pile-up are desired.[8]

Recall that the stair rod has either a pure edge or mixed character (Tables II–IV) and therefore, in the general case, its self-energy E_r is given by:[8]

$$E_r = \frac{L}{4\pi}[K^s_r(b^s_r)^2 + K^e_r(b^e_r)^2]\ln\left(\frac{R}{r_0}\right), \tag{15}$$

where subscript r refers to the stair rod. E_{t1} is composed of two terms: E^{loop}_{t1}, corresponding to the sum of self-energies of each segment and $E^{tr/tr}_{t1}$, corresponding to the interaction energy between the two transverse segments:

$$E_{t1} = E^{\text{loop}}_{t1} + E^{tr/tr}_{t1} \tag{16}$$

E^{loop}_{t1} is:[8,36]

$$E^{\text{loop}}_{t1} = \frac{1}{4\pi}\{L[K^{s,ft}_{t1}(b^{s,ft}_{t1})^2 + K^{e,ft}_{t1}(b^{e,ft}_{t1})^2] + 2.d_1[K^{s,tr}_{t1}(b^{s,tr}_{t1})^2 + K^{e,tr}_{t1}(b^{e,tr}_{t1})^2]\}\ln\left(\frac{R}{r_0}\right), \tag{17}$$

where superscripts s, ft, e, ft, s, tr, e, tr refer to the screw component of the front segment, edge component of the front segment, screw component of the transverse segments, and edge component of the transverse segments, respectively. The transverse segments can be either pure screw or pure edge, yielding two possibilities for $E^{tr/tr}_{t1}$:[8]

$$E^{tr/tr}_{t1} = \begin{cases} -d_1\cdot K^{s,tr}_{t1}\dfrac{(b^{s,tr}_{t1})^2}{2\pi}\ln\dfrac{L}{r_0} & \text{screw segments} \\ -d_1\cdot K^{e,tr}_{t1}\left[\dfrac{(\boldsymbol{b}^{e,tr}_{t1}\otimes\boldsymbol{\xi})\bullet(\boldsymbol{b}^{e,tr}_{t1}\otimes\boldsymbol{\xi})}{2\pi}\ln\dfrac{L}{r_0} + \dfrac{[(\boldsymbol{b}^{e,tr}_{t1}\otimes\boldsymbol{\xi})\bullet\boldsymbol{L}][(\boldsymbol{b}^{e,tr}_{t1}\otimes\boldsymbol{\xi})\bullet\boldsymbol{L}]}{2\pi L^2}\right] & \text{edge segments,} \end{cases} \tag{18}$$

where operators $\otimes$ and $\bullet$ denote cross and scalar products and bold characters denote vectors. Eq. (18) features a special dependence on L. In 2D models, such as that of Mendelson,[3] all energy terms can be normalized with respect to L, but in our 3D model, Eq. (18) prevents this. The energy of the twin fault is given by the product of the loop area and twin boundary energy, Γ^{ijkl}, where $ijkl$ refer to the twinning plane:

$$E_{l1} = \Gamma^{ijkl}\cdot d_1\cdot L. \tag{19}$$

The interaction energy between the stair rod dislocation and the twinning partial dislocation loop is the sum of the interaction energies between the stair rod and each segment (e.g., front and transverse) of the loop. However, in the special case where the stair rod dislocation is pure edge and the transverse twin segments are pure screw, their interaction is null. In fact, it can be shown that for all the dissociation reactions considered here, it is negligible. Therefore, only $E_{r/t1}$ the interaction energy between the stair rod and front segment is accounted for:

$$E_{r/t1} = -L\cdot K^{s,ft}_{t1}\frac{(\boldsymbol{b}_{t1}\bullet\boldsymbol{\xi})(\boldsymbol{b}_r\bullet\boldsymbol{\xi})}{2\pi}\ln\frac{d_1}{r_0} - L\cdot K^{e,ft}_{t1}\left[\frac{(\boldsymbol{b}_{t1}\otimes\boldsymbol{\xi})\bullet(\boldsymbol{b}_r\otimes\boldsymbol{\xi})}{2\pi}\ln\frac{d_1}{r_0} + \frac{[(\boldsymbol{b}_{t1}\otimes\boldsymbol{\xi})\bullet\boldsymbol{d}_1][(\boldsymbol{b}_r\otimes\boldsymbol{\xi})\bullet\boldsymbol{d}_1]}{2\pi d_1^2}\right]. \tag{20}$$

In the case of an $\alpha=2$ dissociation, similar expressions for E_{t2}, E_{l2}, and $E_{t/t2}$ are used for the second twin loop. Because the two twinning dislocations will interact with one another,

TABLE V. Elastic constants for Mg and Zr.

Mg	C_{11}=59.4 GPa	C_{33}=61.6 GPa	C_{44}=16.4 GPa	C_{66}=16.9 GPa	C_{12}=25.6 GPa	C_{13}=21.4 GPa
Zr	C_{11}=143.5 GPa	C_{33}=164.9 GPa	C_{44}=32.1 GPa	C_{66}=35.5 GPa	C_{12}=72.5 GPa	C_{13}=65.4 GPa

two additional contributions are needed: (1) the interaction between the front segments of the two twinning dislocations $E^{ft}_{t1/t2}$ and (2) the interaction between the nonparallel transverse segments $E^{tr}_{t1/t2}$:

$$E_{t1/t2} = E^{ft}_{t1/t2} + 2.E^{tr}_{t1/t2}, \tag{21}$$

where the contributions of each segment type are given by:[8]

$$\begin{aligned} E^{ft}_{t1/t2} = & -L \cdot K^{s,ft}_{t1} \frac{(\boldsymbol{b}_{t1} \bullet \boldsymbol{\xi}^{ft}_{t1})(\boldsymbol{b}_{t2} \bullet \boldsymbol{\xi}^{ft}_{t2})}{2\pi} \ln \frac{d_{\text{twin}}}{r_0} \\ & - L \cdot K^{e,ft}_{t2} \left[\frac{(\boldsymbol{b}_{t1} \otimes \boldsymbol{\xi}^{ft}_{t1}) \bullet (\boldsymbol{b}_{t2} \otimes \boldsymbol{\xi}^{ft}_{t2})}{2\pi} \ln \frac{d_{\text{twin}}}{r_0} \right. \\ & \left. + \frac{[(\boldsymbol{b}_{t1} \otimes \boldsymbol{\xi}^{ft}_{t1}) \bullet \boldsymbol{d}_{\text{twin}}][(\boldsymbol{b}_{t2} \otimes \boldsymbol{\xi}^{ft}_{t2}) \bullet \boldsymbol{d}_{\text{twin}}]}{2\pi d_{\text{twin}}} \right] \end{aligned} \tag{22}$$

and

$$\begin{aligned} E^{tr}_{t1/t2} = & \left[K^{s,tr}_{t1} \frac{(\boldsymbol{b}_{t1} \bullet \boldsymbol{\xi}^{tr}_{t1})(\boldsymbol{b}_{t2} \bullet \boldsymbol{\xi}^{tr}_{t1})}{4\pi} \right. \\ & - K^{s,tr}_{t1} \frac{(\boldsymbol{b}_{t1} \otimes \boldsymbol{b}_{t2}) \bullet (\boldsymbol{\xi}^{tr}_{t1} \otimes \boldsymbol{\xi}^{tr}_{t1})}{2\pi} + \frac{K^{e,tr}_{t1}}{4\pi} [(\boldsymbol{\xi}^{tr}_{t1} \otimes \boldsymbol{e}_3) \bullet \boldsymbol{b}_{t1}] \\ & \left. \times [(\boldsymbol{\xi}^{tr}_{t1} \otimes \boldsymbol{e}_3) \bullet \boldsymbol{b}_{t2}] \right] \cdot I(t1,t2) + \frac{K^{s,tr}_{t1}}{4\pi} [(\boldsymbol{b}_{t1} \bullet \boldsymbol{e}_3) \\ & \times (\boldsymbol{b}_{t2} \bullet e_3)] \cdot J(t1,t2). \end{aligned} \tag{23}$$

Because α=2 dissociations considered here involve two variants of the same twin type, the energy factor of the first and second twinning dislocations are equal. Also, functions I and J depend on segment length and the angle between each segment. These functions are detailed elsewhere.[8] Vectors $\boldsymbol{\xi}^{ft}_{t1}$, $\boldsymbol{\xi}^{ft}_{t2}$, $\boldsymbol{\xi}^{tr}_{t1}$, and $\boldsymbol{\xi}^{tr}_{t2}$ denote the unit vector of the front segments of the first and second twinning dislocation and likewise, the transverse segments of the first and second twinning dislocation. $\boldsymbol{e}_3$ corresponds to the normalized cross product between $\boldsymbol{\xi}^{tr}_{t1}$ and $\boldsymbol{\xi}^{tr}_{t2}$.

E_{prim} is zero when an isolated perfect dislocation dissociates. In the case of a dissociation from an extended partial dislocation (Table III), E_{prim} consists of the energy of the trailing partial dislocation in the glide plane and the stacking fault energy:

$$E_{\text{prim}} = \frac{L}{4\pi} [K^e_{\text{ini2}} (b^e_{\text{ini2}})^2 + K^s_{\text{ini2}} (b^s_{\text{ini2}})^2] \ln \frac{R}{r_0} + \Gamma^{SF} \cdot L \cdot d'_{eq}. \tag{24}$$

The stacking fault area on the slip plane d'_{eq} will be smaller after the dissociation than before since the Burgers vector of stair rod dislocation is smaller than that of the leading partial.

When the dissociation occurs at the head of a pile-up, E_{prim} is that of an $(N-1)$—dislocation pile of length l':

$$\begin{aligned} E_{\text{prim}} = & \Gamma^{SF} \cdot d''_{eq} \cdot L_{\text{ini}} + \frac{L \cdot K^e_{\text{ini}} (b^e_{\text{ini}})^2 (N-1)^2}{4\pi} \ln \frac{4R}{l'} \\ & + \frac{L \cdot K^s_{\text{ini}} (b^s_{\text{ini}})^2 (N-1)^2}{4\pi} \ln \frac{4R}{l'}. \end{aligned} \tag{25}$$

III. RESULTS

A. Application to Mg and Zr

The energetic model for the extension of a nonplanar dissociation is applied to Mg (c/a=1.623) and Zr (c/a=1.593).[37] The room-temperature elastic moduli for these two materials are presented in Table V.[38,39] These are expressed in the usual coordinate system (e.g., c axis defines axis 3). They are directly used for calculating K^e and K^s for the slip and stair rod dislocations in the basal plane. For the prismatic or twinning planes, the stiffness tensor needs to be transformed to calculate K^e and K^s.[8] Table VI summarizes K^e and K^s for dislocations in the basal plane and all seven twinning planes for Mg and Zr. In all cases, $K^e > K^s$, and hence, energy contributions of edge segments will be larger than those of screw segments of the same length. The same trend is found on the prismatic plane.

For Mg, Γ^{SF}=14 mJ m^{-2} in the basal plane is extracted from Baskes *et al.*,[40] which lies at the upper range of values predicted for Γ^{SF} of type I_2: 8–14 mJ m^{-2}.[41]

As is the case in nearly every twin nucleation theory, our model finds that in some cases Γ^{ijkl} is important. Unfortunately, Γ^{ijkl} is difficult to measure and is best estimated from

TABLE VI. Energy prefactors for Mg and Zr.

Unit: mJ/mm^3		Bas.	Bas. 60°	$(\bar{1}011)$	$(\bar{1}012)$	$(\bar{1}013)$	$(\bar{2}111)$	$(\bar{2}112)$	$(\bar{2}113)$	$(\bar{2}114)$
Mg	K^e	24.6	25	24.5	24.7	24.8	24.1	24.2	24.2	24
	K^s	16.7	16.7	17.6	17.3	17	16.9	17.7	18	16.9
Zr	K^e	54	57.6	55.4	56.4	56.8	53.2	53	53	52.8
	K^s	33.7	33.7	37.2	36.1	35.3	34.1	37.2	38.6	34.1

TABLE VII. Materials constants for Mg and Zr.

Mg	$\Gamma^{10\bar{1}1}=143$ mJ/m^2	$\Gamma^{10\bar{1}2}=189$ mJ/m^2	$\Gamma^{10\bar{1}3}\approx 189$ mJ/m^2	$\Gamma^{\bar{2}111}=148$ mJ/m^2	$\Gamma^{\bar{2}112}=145$ mJ/m^2	$\Gamma^{\bar{2}113}\approx 145$ mJ/m^2
	$\Gamma^{\bar{2}114}\approx 145$ mJ/m^2	$R=1.E-6$ m	$r_0=a$	$c=0.52$ nm	$a=0.32$ nm	$\Gamma^{SF}=14$ mJ.m^{-2}
Zr	$\Gamma^{10\bar{1}1}=225$ mJ/m^2	$\Gamma^{10\bar{1}2}=262$ mJ/m^2	$\Gamma^{10\bar{1}3}\approx 262$ mJ/m^2	$\Gamma^{\bar{2}111}=169$ mJ/m^2	$\Gamma^{\bar{2}112}=245$ mJ/m^2	$\Gamma^{\bar{2}113}\approx 245$ mJ/m^2
	$\Gamma^{\bar{2}114}\approx 245$ mJ/m^2	$R=1.E-6$ m	$r_0=a$	$c=0.514$ nm	$a=0.32$ nm	$\Gamma^{SF}=14$ mJ.m^{-2}

first-principle calculations or atomistic simulations with reliable potentials.[27,28] On the other hand, the values reported for Mg from both methods are reasonably consistent with little variation despite different potentials and methods. Because the works of Serra and Bacon[27] provide the most values from a single potential (a many-body potential fitted to Mg), we use them in the following Mg calculations, unless stated otherwise. Table VII lists the Γ^{ijkl} values used for Mg. For some twinning planes, $(\bar{1}013)$, $(\bar{2}113)$, and $(\bar{2}114)$, Γ^{ijkl} had to be assigned as no estimates are provided in the literature. Values of Γ^{ijkl} for Zr are also extracted from simulations by Serra and Bacon[42] and reported in Table VII. The effect of varying Γ^{ijkl} will be addressed later in the discussion.

The outer cutoff radius R (see Table VII) was chosen to be 1 μm, which is the order of the grain size in coarse-grained Mg and Zr. We find that the calculations are not very sensitive to R.

The inner cutoff radii r_0 depends on the type of dislocation considered and energies are sensitive to r_0. Until more quantitative knowledge of dislocation core sizes and activation energies can be obtained, we set $r_0=a$, a reasonable value for all single dislocation segments, and neglect any dependencies on screw-edge or zonal character.

1. Dissociations from a single dislocation

The evolution of E/E_{ini} given by Eq. (9) in an Mg single crystal upon dissociation from an individual dislocation into twinning dislocations is studied first. Figure 4 presents typical curves for E/E_{ini} versus d/r_0 for some dissociations onto the $(\bar{1}012)$ twinning plane. As shown, E/E_{ini} rises linearly with d and no stable twin fault with $d_s>2r_0$ is created. The same calculations were performed for all dissociations in Tables II–IV and they yielded the same result: a distinguishable twin fault loop was not produced. Apparently, in every case, the attractive forces between the twinning dislocations and the other products are too high, and the core stays compact. Note that in some reactions, E/E_{ini} starts below unity at $d=2r_0$ [for instance in Figs. 4(a) and 4(b)]. This simply means that the total energy of the product dislocations is lower than that of the original slip dislocation, but it does not imply that the dissociation is favorable for twin loop production.

Figure 4(a) shows the effect of varying τ_{t1}—the stress assumed to cause the initial split—on the $\alpha=1$ dissociation of a perfect basal dislocation of length $L=10$ nm. [Since a single dissociation ($\alpha=1$), is considered, τ_{t2} needs not to be considered.] As shown, τ_{t1} has no effect on the evolution of E for small d. Most importantly, a twin fault of $d_s>2r_0$ cannot be induced by simply increasing τ_{t1}, even to the highest value 1280 MPa. This results, because the self-energies and the interaction energies between dislocations segments that dominate the energetics for small d are independent of τ_{t1}. τ_{t1}, however, affects E evolution in the range of large d. As shown, the rate at which E grows with d reduces as τ_{t1} increases. This occurs because the increase in W compensates for the increase in twin fault energy E_l, both of which grow linearly with d.

Even if enough stress or energy was supplied to split the slip dislocation into twinning dislocations, the attractive forces supplied by the twin fault and interactions with other product partials prevent a suitably wide extension. Calculations for d_s that follow can, therefore, prove meaningful in spite of limited knowledge of the necessary resolved stress to activate a dissociation event or E_{activ} and henceforth, $\tau_{t1}=\tau_{t2}=0$ MPa without loss of generality.

Recall that our 3D treatment engenders a size effect. The dependence on L enters in the interaction energy term between two transverse segments of the twin loop. Figures 4(b) and 4(c) compares the effect of varying L from 5 to 20 nm for dissociations of basal and prismatic dislocation, respectively, onto the $(\bar{1}012)$ twin plane. As shown, L affects the evolution appreciably for prismatic dissociations and insignificantly for basal dissociations. The reason is that the interaction energy between the two transverse edge segments in the twin loop produced by the prismatic dissociation is higher than that between the two transverse screw segments in the loop produced by the basal dissociations.

Although an interesting size effect, changing L does not alter the ability of the dissociation to produce suitably sized twin fault loops $d_s>2r_0$. Because this is our focus, $L=10$ nm in the remainder of our calculations.

Fig. 5 compares the energy for dissociations of basal or prismatic dislocations into twinning dislocations on the seven twin planes: (a) $\alpha=1$ dissociations of a perfect basal, (b) $\alpha=2$ dissociations of a perfect basal, (c) $\alpha=1$ dissociations of a basal partial, and (d) $\alpha=1$ dissociations of a perfect prismatic. Regardless of the twin plane, no stable twin fault $d_s>2r_0$ is produced. Note that $d_s=2.1r_0$ in the cases of (a) single and (b) double dissociation from a perfect basal dislocation onto the $(\bar{2}114)$ and the $(\bar{1}013)$ planes is still too small to be considered a distinguishable twin fault loop.

In spite of the failure of dissociations of isolated dislocations to produce a stable twin fault, a few important conclu-

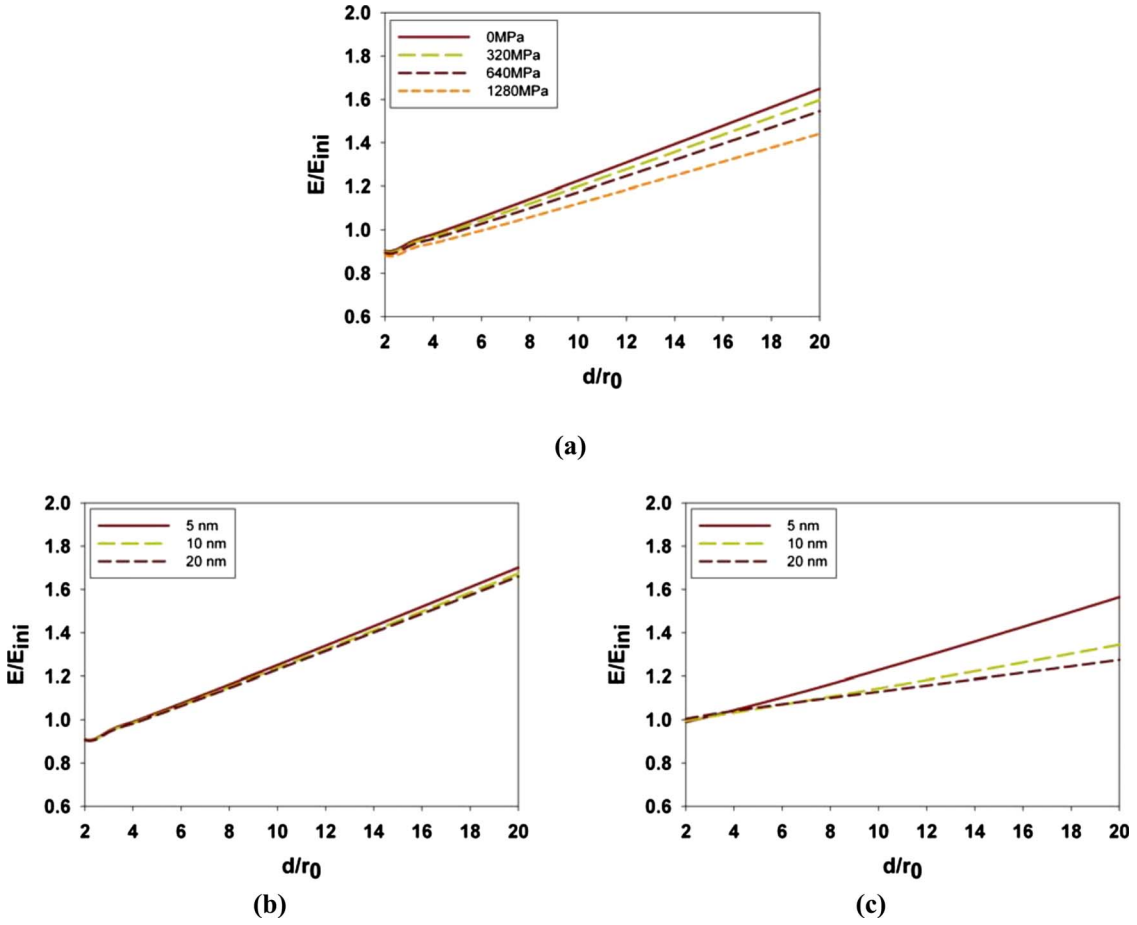

FIG. 4. (Color online) (a) Effect of applied stress τ and (b) segment length L on the evolution of the system free energy E during the single dissociation of a perfect basal dislocation onto the $(\bar{1}012)$ plane; (c) effect of L on the evolution of E during the dissociation of a prismatic $\langle a \rangle$ dislocation onto the $(\bar{1}012)$ plane.

sions can be drawn regarding their energetics. First, compared to a single ($\alpha=1$) dissociation, a double ($\alpha=2$) dissociation involves a larger initial energy drop (smaller initial E/E_{ini}) immediately after the dissociation, due to its lower strength stair rod dislocation, but a higher rise in energy thereafter due to the formation of two faults instead of one. This is seen, for example, by comparing Figs. 5(a) and 5(b) for the same twin type. Second, dissociations from an extended basal dislocation, Fig. 5(c), lead to slightly lower, but otherwise similar, energy states than those of a perfect basal dislocation. Comparing Fig. 5(a) and 5(c) shows that this result holds for all twin types. Further examination in Fig. 6 of the evolution of individual contributions, namely E_r, E_{l1}, $E_{r/t1}$, E_{t1}^{loop},$E_{t1}^{tr/tr}$, and E_{prim}, after dissociations of (a) perfect and (b) partial basal dislocations into $(\bar{1}012)$ twinning dislocations explains the insensitivity. While the stair rod contribution is reduced for the partial case, its glide plane energy E_{prim} is enhanced. Next, unlike the basal dislocations, dissociations from prismatic dislocations show a preference for extending on the $(\bar{2}11X)$ planes rather than $(\bar{1}01X)$ planes [Fig. 5(d)]. This preference results from the fact that the interaction between the stair rod dislocation and the edge parts of the twinning dislocations (denoted as $E_{r/t1}$—edge contribution) are more repulsive in the $(\bar{2}11X)$ case than in the $(\bar{1}01X)$ case. As an example, Fig. 7 compares the evolution of individual components involved in dissociations from prismatic dislocations onto (a) $(\bar{2}111)$ and (b) $(\bar{1}012)$ planes for Mg. The (negative) interaction energy of the "$E_{r/t1}$—edge contribution" is greater in the former than latter. This difference is small for dissociations of a lone slip dislocation, but as we show later, it will become magnified when the dissociation occurs at the head of a pile-up.

Fourth, interaction energies dominate when the twin loop is a few times r_0 ($<10r_0$), but the twin boundary energy E_{lt} dominates when the loop grows much larger than r_0, leading to the linear growth in E with d. Figures 6 and 7 make clear that selecting an abnormally small Γ^{ijkl} (small compared to that given by *ab initio* calculations) does not suffice to stabilize a twin fault loop. The contribution of Γ^{ijkl} quickly dominates all other contributions, apart from the stair rod. For example in Figs. 6(a) and 7(b), Γ^{ijkl} dominates immediately and in Fig. 6(b) and 7(a), it dominates in the neighborhood of ~ 5 nm. Last, Figs. 6 and 7 also show that the only contribution that lowers the energy of the system is the interaction energy between the stair rod and the twinning dislocation. This contribution increases as the angle θ (see Fig. 2) between the basal plane and the twinning plane decreases and the Burgers vectors of these two dislocations become more aligned. In this respect, lower c/a ratios and twin planes

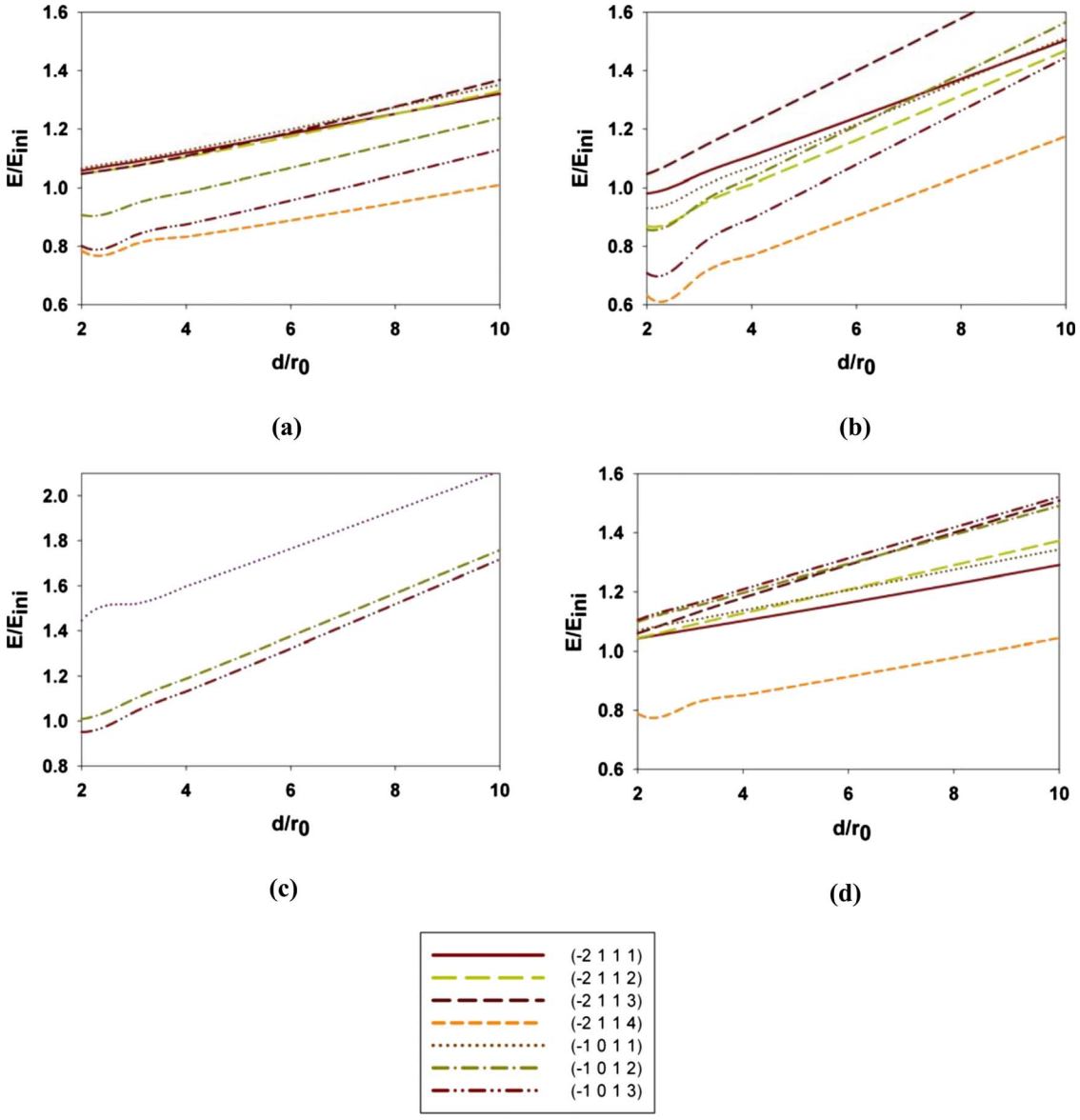

FIG. 5. (Color online) Evolution of the free energy during (a) the single dissociation of a perfect basal dislocation, (b) the double dissociation of a perfect basal dislocation, (c) the single dissociation of an extended basal dislocation, and (d) the single dissociation of a perfect prismatic dislocation.

$(\bar{1}013)$ and $(\bar{2}114)$ would lead to lower total energies (the latter effect is seen in Fig. 5) than the other twin planes.

Before examining the influence of a pile-up, we would like to distinguish between the results presented in this section and those predicted by Mendelson.[3,13] Although this study is based on the same dissociation reactions, the energetic treatments are different. The present analysis is fully three-dimensional and thus considers additional interactions and introduces a dependence on L. It is not based solely on a force balance between the twin boundary energy and interaction forces of the dissociation products at a fixed separation (a in the case of Mendelson). It provides a method for calculating a twin fault loop of size d_s. Therefore our model is expected to lead to different conclusions that those of Mendelson. For example, using the twin boundary energies in Table VII, Mendelson's criterion would predict that the single dissociation of a perfect basal $\langle a \rangle$ dislocation onto the $(\bar{2}114)$ twinning plane is favorable, but our analysis would not. Indeed the main result of our analysis is that in fact that none of these dissociations lead to a stable twin fault loop ($d_s > 2r_0$), regardless of twin fault energy, L, and slip dislocation type or character.

2. Dissociations from a pile-up

Our calculations find that a pile-up changes the energy and stability of the dissociated core. In the presence of a pile-up, it is possible that a double ($\alpha=2$) dissociation will not extend symmetrically $d_1 \neq d_2$ (Fig. 8). Take, for example, the case of a perfect basal dislocation splitting onto the $(\bar{1}012)$ plane. Figure 9(a) shows a three-dimensional map of

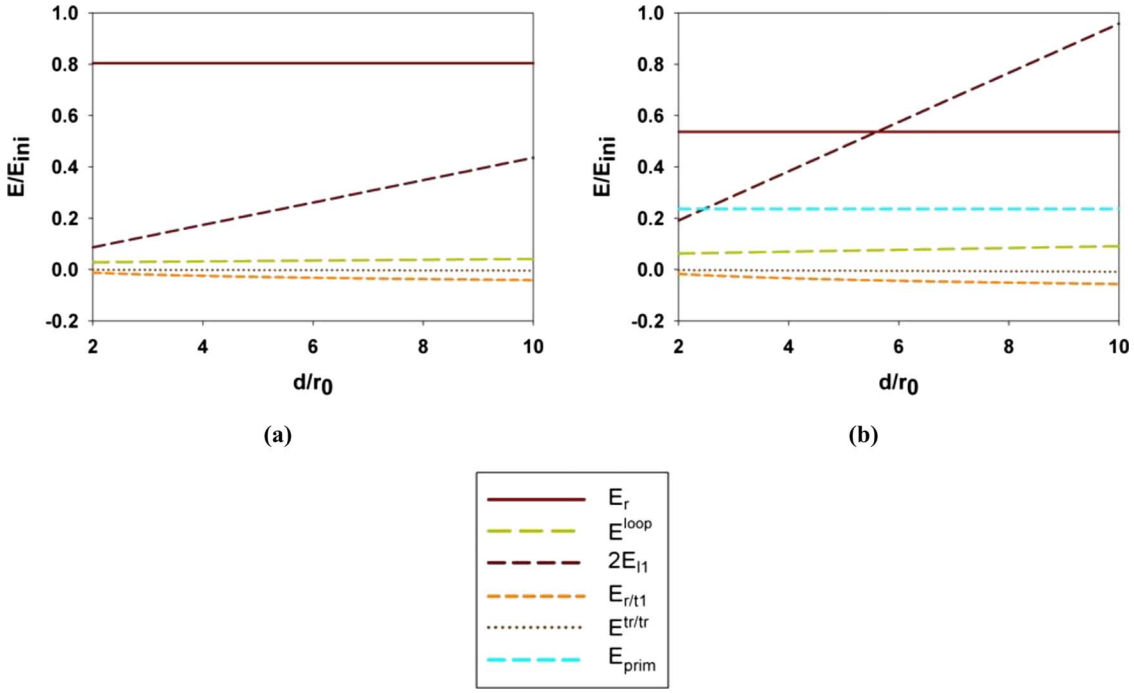

FIG. 6. (Color online) Evolution of the individual energy contributions during a spontaneous dissociations from a 10 nm long dislocation: (a) single dissociation of a perfect dislocation from the basal plane to the $(\bar{1}012)$ plane, (b) single dissociation from a basal partial dislocation to the $(\bar{1}012)$ plane.

E/E_{ini} versus the variable set d_1 and d_2 in the presence of an $N=15$ pile-up of basal dislocations. The solid curves in Fig. 9(b) are certain cross sections of the map in Fig. 9(a). An asymmetric double dissociation favoring propagation of b_{t1} in d_1 while b_{t2} remains fixed at a small d_2 is more energetically favorable than a symmetric one $(d_1=d_2)$ or an asymmetric double dissociation favoring the propagation of b_{t2} over b_{t1}.

For comparison, the dashed curve is the analogous case of a single $(\alpha=1)$ dissociation with the same pile-up. As found before for dissociations of isolated dislocations, an $\alpha=2$ dissociation requires more energy than an $\alpha=1$ dissociation.

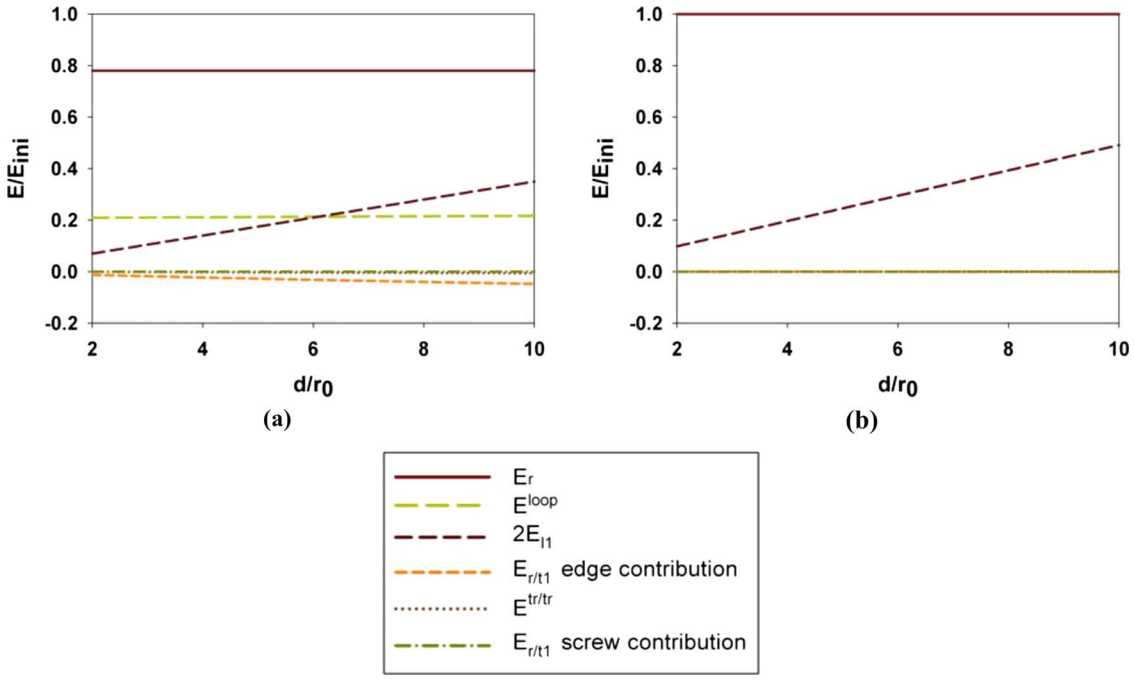

FIG. 7. (Color online) Evolution of the individual energy contributions during the following spontaneous single dissociations from a 10 nm long perfect prismatic dislocation: (a) onto the $(\bar{2}111)$ plane, (b) onto the $(\bar{1}012)$ plane.

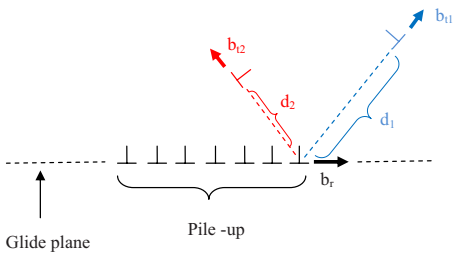

FIG. 8. (Color online) Schematic of an asymmetric double dissociation from a dislocation pile-up.

However, as shown in Fig. 9(b), the difference is more pronounced in the case of a pile-up.

More importantly, in the two most favorable cases, an asymmetric ($\alpha=2$) dissociation (blue solid) or an $\alpha=1$ dissociation into b_{t1} (blue dash), a stable loop d_s of sufficient size is created. The reason for this is explained in Fig. 10. As revealed in Fig. 10, the interaction between the pile-up and b_{t1} is repulsive (negative interaction energy), while that between the pile-up and b_{t2} is attractive (positive interaction energy). Accordingly a dissociation from a pile-up can lead to one stable twin fault d_s but not two, and d_s increases in size as N increases.

Based on these results the remainder of the paper focuses only on the most favorable mechanism: $\alpha=1$ dissociations of the lead dislocation of an N-sized pile-up ($N \gg 1$) containing the same types of dislocations (same orientation, same Burgers vector, etc.).

The effect of an $N=10$ dislocation pile-up of basal dislocations on the dissociation of its leading one into twinning dislocations on the $(\bar{2}11X)$ and $(\bar{1}01X)$ planes for Mg is shown in Figs. 11(a) and 11(b), respectively. From these reactions, stable twin loops of $d_s \sim 2$ to ~ 6 nm are found. In Fig. 11(a), formation of a loop on the $(\bar{2}113)$ plane is the most favorable followed by $(\bar{2}112)$ in terms of lower total energy and larger d_s.

In these cases, a pile-up contributes to twin fault loop formation because of the repulsive forces provided its stress field on the twinning dislocations, not because of stress concentrations. Only dissociations that produce twinning dislocations that are directed away from the pile-up will likely form a stable fault loop because of the pile-up. This implies that $\alpha=1$ dissociations without the repulsive pile-up/twin interaction will not produce a stable loop regardless of N. To demonstrate this point, Fig. 12 shows a dissociation of the lead dislocation of a pile-up of $N=10$ prismatic dislocations onto the $(\bar{1}01X)$ planes for (a) Mg and (b) Zr. Because of the negligible interaction between the remaining prismatic dislocations in the pile-up and the $(\bar{1}01X)$ twinning dislocations, no stable loops are created. It can be shown that larger N does not change this result.

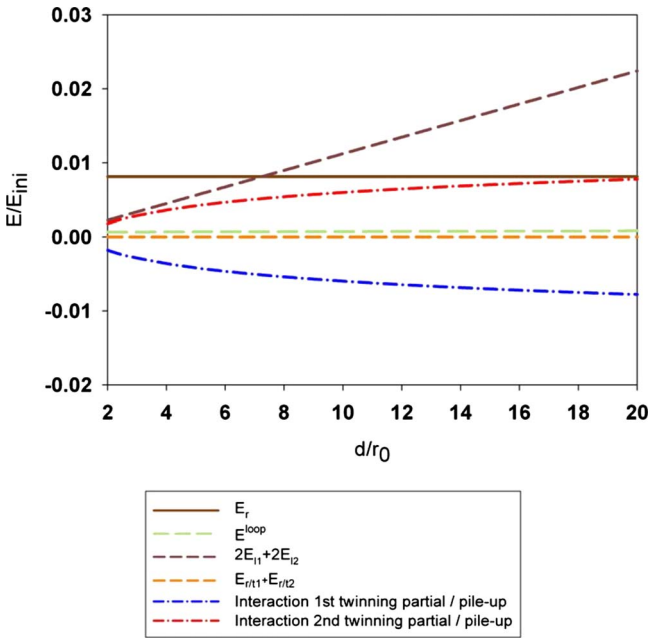

FIG. 10. (Color online) Evolution of the individual energy contributions during a symmetric (e.g., $d_1=d_2$) double dissociation from a perfect basal dislocation onto the $(\bar{1}012)$ plane.

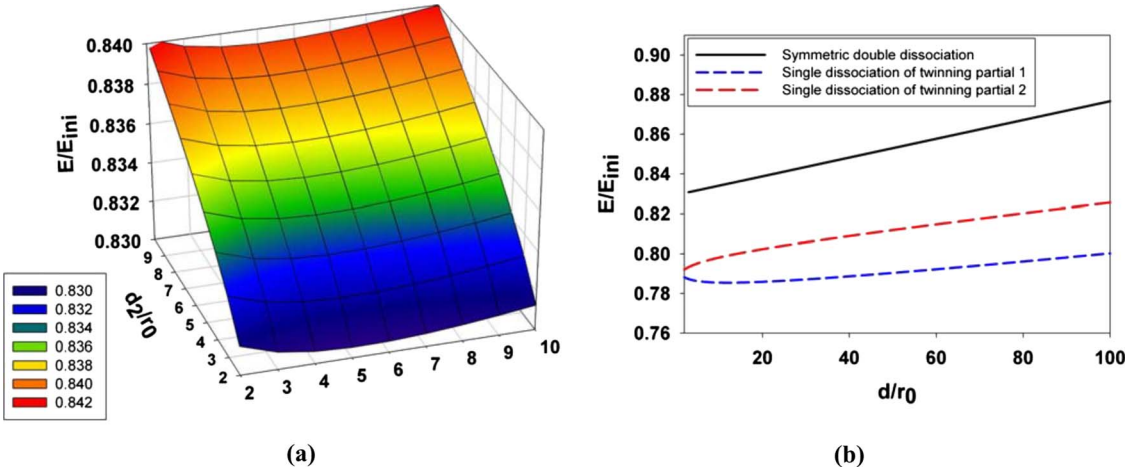

FIG. 9. (Color online) (a) Three-dimensional mesh of the energy evolution during the double dissociation of a perfect basal dislocation onto the $(\bar{1}012)$ plane. (b) Comparisons of certain cross sections of the 3D mesh, namely a symmetric and symmetric double dissociations (solid curves) and a single dissociation (dash).

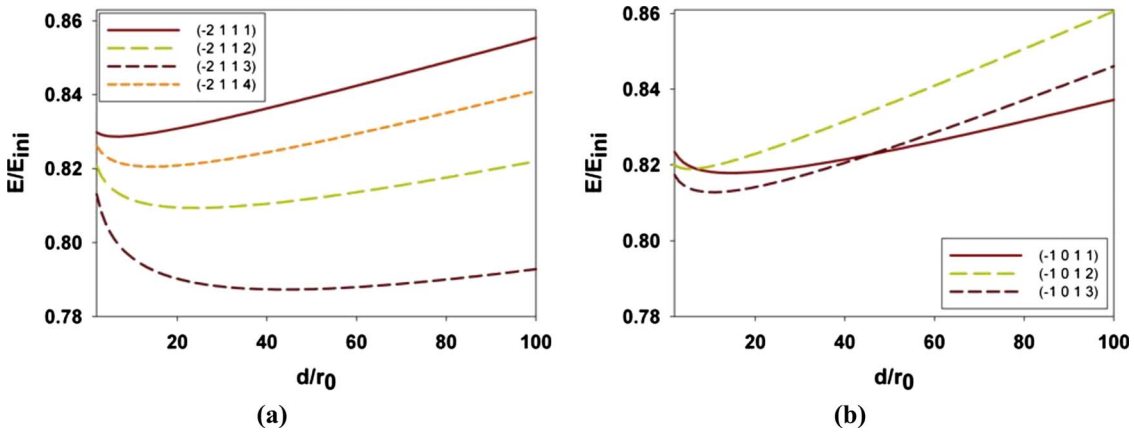

FIG. 11. (Color online) (a) Energy evolution during the single dissociation from a perfect basal dislocation ahead of a ten basal dislocation pile-up onto the $(\bar{2}11X)$ twin planes, (b) energy evolution during the single dissociation of a perfect dislocation at the head of a ten dislocation pile-up on the basal plane for the $(\bar{1}01X)$ twin modes.

The interaction between prismatic dislocations and $(\bar{2}11X)$ twinning dislocations, however, is repulsive. Figure 13 shows the energetics of dissociation from a pile-up of ten prismatic dislocations onto the $(\bar{2}11X)$ planes for (a) Mg and (b) Zr. As expected, for both metals, the dislocation pile-up produces a stable twin fault loop, which is larger for Zr than Mg for the same twin type. Significant differences in the interactions between prismatic dislocations and a $(\bar{1}01X)$ versus $(\bar{2}11X)$ twinning dislocation loop is found in their interaction with the transverse segments of the loop; such differences would not be predicted in the 2D case.[13]

IV. DISCUSSION

A. Effect of number of dislocations in the pile-up and sensitivity to the twin boundary energy

Figure 14 presents the evolution of d_s for the dissociation of a basal $\langle a \rangle$ dislocation onto the $(\bar{1}012)$ plane with N for three different values of Γ: $0.8\Gamma_{\text{ref}}$, Γ_{ref}, $1.2\Gamma_{\text{ref}}$, where Γ_{ref} is the value reported in Table VII for Mg. Results show that d_s increases linearly with N at a rate which decreases with Γ. In other words, it becomes easier to generate a twin fault loop of a given size when Γ is low. Also note that a large pile-up is not necessary; d_s reaches a reasonable value on the order of $\sim 10-15 r_0$ for a relatively small pile-up containing only ~ 10 dislocations.

B. Two distinctive roles of the pile-up

This work shows that an N-dislocation pile-up of suitable size is necessary (but not sufficient) to form a stable twin fault by a nonplanar dissociation of an $\langle a \rangle$ slip dislocation. The pile-up dissociation model developed here can determine if it will form and if so, its size d_s for a given N. For reactions in which the interaction force between the slip and twinning dislocations is repulsive, a pile-up, or any suitable defect arrangement, can help its lead dislocation dissociate and form a stable twin fault loop an order of magnitude greater than r_0. For this class of reactions, both N and Γ have an influence on d_s. For the other class of reactions in which there is no such repulsive force, no value of fault energy or N can successfully produce a stable twin fault.

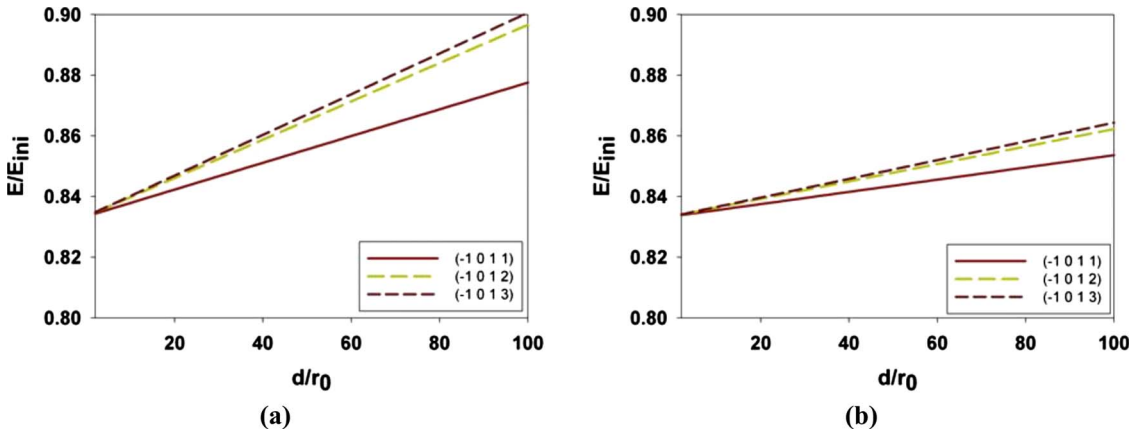

FIG. 12. (Color online) Energy evolution during the single dissociation of a perfect prismatic dislocation ahead of a ten prismatic dislocation pile-up for the $(\bar{1}01X)$ twin modes in (a) Mg and (b) Zr.

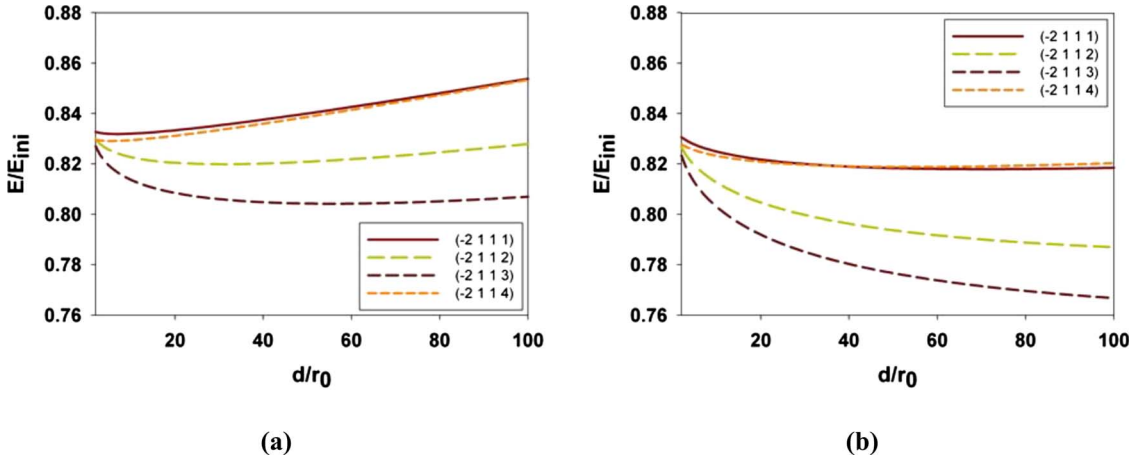

FIG. 13. (Color online) Energy evolution during the single dissociation of a perfect prismatic dislocation ahead of a ten prismatic dislocation pile-up for the $(\bar{2}11X)$ twin modes in (a) Mg and (b) Zr.

It is important to emphasize that the pile-up has two roles. Before the dissociation, it can supply the stress needed for the dissociation, such as $N\tau$. After the dissociation it helps the twinning dislocations overcome any attractive forces and reach a stable extension sufficiently far away from the reaction center. The former role is the one considered in virtually every previous twin nucleation model.[3,8,11,13,17,43] In the first role, the larger the pile-up the more likely is the dissociation event, regardless of $\alpha=1$ or 2 or the slip or twinning dislocations involved. In contrast, in the role that the pile-up plays here, a pile-up only favors creation of one twin fault loop, not two, and only for some reactions. In these cases, it is significant to point out that small pile-ups suffice. Smaller pile-ups, compared to larger ones, are easier to form and more likely to form especially in high strain rate and low-temperature conditions where twins are known to prevail. (The same can be said of low stacking fault energy metals.) They are also more likely to be found anywhere in the grain, not just at the grain boundaries and other strong obstacles. Dislocations most often move in arrays and not singly.

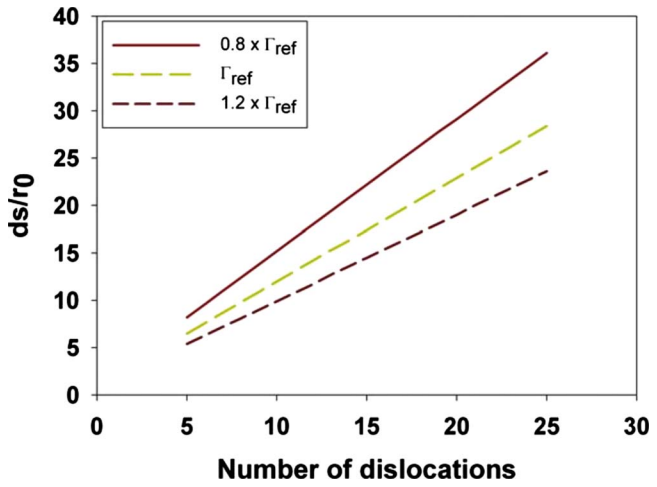

FIG. 14. (Color online) Evolution of the stable twin nucleus size d_s during the single dissociation from a perfect basal dislocation onto the $(\bar{1}012)$ twin plane, as a function of the number of dislocations within a pile-up N for three different values of the twin boundary energy.

To neglect the second role would lead to inaccurate results. In doing so, for instance, Mendelson concluded that all unfavorable reactions (single, double, triple dissociations, etc.) would become favorable in the presence of a pile-up of sufficient size. As shown here, this conclusion is incorrect.

C. Possible mechanisms for twin growth from a twin fault loop

After a twin fault loop of sufficient size d_s is created, there are several possible outcomes. On one hand, the small fault may actually be the twin nucleus and the twin can grow directly from it. On the other hand, it may be the first of many consecutive layers that constitute a twin nucleus. The multilayer structure would, in this case, require subsequent creation of partials of perhaps differing or equal Burgers vector. Once a nucleus is formed, twin growth processes can commence, the criterion of which would be related to the forces needed to move the twinning dislocation in its twin direction away from the stair rod, resisting the attractive forces of the fault (or faults in a multilayer case) and interactions with the remaining dissociation products and surrounding defects. If such is the case, fault expansion or successive layers may form in several ways. As suggested for fcc twins,[44] it is possible that several twin nuclei, whether single layer or multilayer, could coalesce to grow a twin. Also, the same dissociation that created the initial fault d_s may simply be repeated in adjacent planes under the same local stress state. It has also been proposed that the residual stair rod left from the first dissociation can successively produce more twinning dislocations, as long as the first twinning dislocation glides sufficiently far away.[3,13] Accordingly, if the first fault loop can expand, the residual stair rod left from the first dissociation would act as a twin source. As considered crystallographically by Yoo,[45] as well as predicted in molecular simulations,[26,29] slip dislocations can react with the already formed fault boundary and produce more twinning dislocations which then laterally propagate the twin

front. Another method of growth, which has yet to be observed in hcp metals, could be the creation of twinning dislocation dipoles in adjacent layers of the twin nuclei seen in dynamic simulations of bcc metals using MD and discrete lattice methods.[4,23] Nevertheless, in every case, once the first twin fault is formed, fault production in neighboring layers requires less energy as no new fault area is created.

In light of the discussion above, if one must identify one, a critical twinning stress would be more appropriately associated with the stress to split, or else, to grow from a stable fault loop d_s after it has formed. These two events appear to be more sensitive to stress than d_s. The former would not be related to a resolved stress, but the latter would. If a dissociation and hence, twin nucleation is to be activated by stress, a local effective shear stress should be used, and not solely the applied one.

D. Effect of slip dislocation sources and mobility

Orientation imaging microscopy on polycrystalline Zr and Mg shows that twins, of micron-scale thickness or larger, are connected to grain boundaries.[46,47] Based on the pile-up dissociation model presented here, in order for a twin to emanate from the grain boundary into the interior, the head of the pile-up must face toward the interior. In the work of by Murr and Wang,[48] such interior-facing pile-ups have been observed via TEM in Ni and stainless steel. They show that the spatial distribution of sessile dislocations after light straining (e.g., $\varepsilon < 0.02$) is inhomogeneous, and the dislocation density near grain boundaries is much higher than in the interior. Most importantly, in this premacro yield region, grain boundaries emitted dislocation "profiles"—which the authors stated resemble and may act as pile-ups—directed toward the grain interior. In fact, the presence of such pile-ups had been suggested earlier in the pioneering work by Li.[49] If the lead dislocation at the head of one of these interior-facing pile-ups were to dissociate, then it would result in twin nucleation and subsequent propagation into the interior. Twin nucleation would then be dependent on: (1) the activation of grain-boundary dislocation emission, which is related to grain-boundary misorientation, and (2) the competition between dislocation dissociation and other mechanisms (e.g., cross slip, climb).

Regarding (2), rather than dissociating, a dislocation could instead, for example, cut through the obstacle or change glide plane via climb or cross slip. The former is expected in the case of edge dislocations and the latter in the case of screw dislocations. The selected mechanism is necessarily the most energetically favorable mechanism. Consider, for instance, the case of the competition between dislocation climb and dislocation dissociation, which is particularly relevant to the case of basal $\langle a \rangle$ dislocation exhibiting either a pure edge or a mixed character. Let ΔG_{twin} and ΔG_{climb} denote the Gibbs free energies associated with a twin nucleation and a dislocation climb event, respectively. Each mechanism is activated if sufficient energy is provided to overcome its corresponding activation barrier:

$$\Delta G_{\text{twin}} - \tau_{\text{twin}}^{\text{eff}} \nu_{\text{twin}} \leq 0$$

and

$$\Delta G_{\text{climb}} - \tau_{\text{climb}}^{\text{eff}} \nu_{\text{climb}} \leq 0, \tag{24'}$$

where ν_{twin} and ν_{climb} are the activation volumes for twin nucleation and dislocation climb, and $\tau_{\text{twin}}^{\text{eff}}$ and $\tau_{\text{climb}}^{\text{eff}}$ are the effective resolved shear stresses, respectively, on the twin plane and on the plane perpendicular to the glide plane. ("Effective" in this case signifies that the stress is due to a combination of the applied stress and that generated dislocation pile-up.) Twin nucleation will be preferred to dislocation climb if:

$$\frac{\nu_{\text{climb}} \Delta G_{\text{twin}}}{\nu_{\text{twin}} \Delta G_{\text{climb}}} \leq \frac{\tau_{\text{twin}}^{\text{eff}}}{\tau_{\text{climb}}^{\text{eff}}}. \tag{25'}$$

A similar procedure can be applied to any mechanism, such as cross slip, competing with twin nucleation.

A discussion of completing mechanisms with energetic barriers is not complete without considering temperature effects. The values of ΔG for each possible mechanism (e.g., dissociation, climb, cross slip, etc.) can vary differently with temperature. First of all, the size of a dislocation pile-up generally increases as temperature decreases, promoting twin nucleation. Second, at lower temperatures, twin nucleation activity would be favored over other mechanisms, such as climb or thermally-activated cross slip, that are well known to become more difficult as temperature decreases. Also, cutting-through events may be less likely at lower temperatures. As shown in early work by Tomé and Savino,[50] the interaction energy between a point defect—which could act as a pinning point leading to a dislocation pile-up—is higher at lower temperatures. Interestingly they find that this effect is more pronounced in the case of Zr than for Mg. Therefore, compared to cut through, twinning may be more favorable at lower temperatures and for Zr than Mg. Finally, it is conceivable that the Gibbs free enthalpy—defined as the difference between the activation enthalpy and the product of the temperature and the activation entropy—associated with dislocation dissociation could decrease with decreasing temperature, again, favoring twin nucleation at lower temperatures. Reductions in the Gibbs free enthalpy with decreasing temperature have been measured experimentally in several metals, such TiAl (Ref. 51) and in high-entropy alloys,[52] for temperatures ranging from 78 to 398 K. A similar trend was measured in the case of thermally-activated relaxation of zirconium-oxygen single crystals.[53] At every temperature, the dissociation will be accompanied by an increase in entropy. However, it is reasonable to expect that this increase will be small at larger temperatures, where there is much more disorder, and large at lower temperatures, where there is much less. At this stage, this last idea is pure speculation.

E. Relationship to observations

Plastic deformation in Mg occurs primarily via basal slip and $(\bar{1}012)$ twinning.[54,55] As shown here, dislocation pile-ups on the basal plane can lead to favorable twin nucleation on both $(\bar{2}11X)$ and $(\bar{1}01X)$ planes. Determining which of these twinning planes is selected depends on their corresponding activation barriers, parameters which cannot be accessed by linear elasticity. Decomposition of the core of the initial dis-

location is an inelastic process, not accounted for in the present model. The energy of the initial slip dislocation core and those of the product dislocations (including twinning partials) after the dissociation will determine the activation energy, and hence, the likelihood of nucleating one twin type over another. Atomistic calculations, on the other hand, have the potential to assess the feasibility of the dissociations studied here. In future work, we will apply atomistic calculations to estimate activation barriers and further study the feasibility of twin nucleation via nonplanar dissociations.

In pure Zr, the most common twin type is $(\bar{1}012)$, observed from liquid nitrogen (76 K) to room temperature.[56] Additional twin types observed at temperatures from 76 to 150 K, are $(\bar{2}112)$ and $(\bar{2}111)$.[2] As shown here, dissociations from prismatic dislocation pile-ups, which were observed experimentally,[57] can only provide $(\bar{2}11X)$ twins and not $(\bar{1}01X)$ twins. Although not shown specifically for Zr, dissociations from basal dislocation pile-ups can, however, provide $(\bar{1}01X)$ twins. Unfortunately, basal slip is not expected in pure Zr at least at room temperature, low strain rates, and moderate strain levels.[2] However, the present calculations show that only moderate dislocation activity, i.e., a ten-dislocation pile-up, is required for twin nucleation to be activated, and basal slip at this level is certainly possible, as observed by Bailey,[57] and later by Dickson and Craig.[58] Thus, basal slip in Zr could still serve as a triggering mechanism for $(\bar{1}012)$ twinning. Otherwise, another mechanism may operate, such as dissociations from $\langle c \rangle$ dislocations or $\langle c+a \rangle$ dislocations.[13]

V. CONCLUSIONS

Twin nucleation by a nonplanar dissociation of slip dislocations is studied by means of continuum linear elasticity dislocation theory. The proposed model calculates the energy and stable extension after the dissociation, accounting for the elastic anisotropy of the medium, the three-dimensional aspects of a twin dislocation loop, and all possible energetic contributions. Dissociations may initiate from either prismatic or basal $\langle a \rangle$ slip dislocations, or partial basal dislocations, and lead to one or two twinning dislocations on noncoplanar planes. It is shown that, regardless of the applied stress to trigger the dissociation, twin fault energy, and length of slip segment, a dissociation from a lone dislocation, either a perfect one or Shockley partial, is not likely to lead to a stable twin fault loop larger than $2r_0$ the core width of an initial slip dislocation. Instead after the dissociation, the cores remain compact due to strong attractive forces between the dissociation products.

With the addition of a pile-up of slip dislocations, these same calculations elucidate a new mechanism based on the dissociation of its lead slip dislocation. If repulsive forces exist between the dislocations remaining in the pile-up and the product twinning dislocation, then this dissociation can produce a distinguishable twin fault loop, much greater than r_0. Using this criterion, it is shown that dissociations produce one fault loop, not two, even when it is crystallographically possible to produce two noncoplanar loops. All dissociations from the basal plane can result in stable twin fault loops. On the contrary, dissociations from the prismatic plane lead to stable twin faults only in the case of dissociations onto the $(\bar{2}11X)$ planes. The calculations begin after the dissociation, and therefore the feasibility of this mechanism still relies on knowledge of the activation barrier for the dissociations. Finally, we conjecture that a dependence on slip dislocation pile-ups implies that twin nucleation will, indirectly, be rate-dependent, and particularly favorable when thermally-activated dislocation glide is restricted.

ACKNOWLEDGMENTS

The authors wish to thank Carlos N. Tomé for insightful discussions and a careful reading of this draft. This work was supported by the Office of Basic Energy Science Project FWP 06SCPE401.

[1] J. W. Christian and S. Mahajan, Prog. Mater. Sci. **39**, 1 (1995).
[2] G. C. Kaschner, C. N. Tome, R. J. McCabe, A. Misra, S. C. Vogel, and D. W. Brown, Mater. Sci. Eng., A **463**, 122 (2007).
[3] S. Mendelson, Mater. Sci. Eng. **4**, 231 (1969).
[4] S. Ishioka, J. Appl. Phys. **46**, 4271 (1975).
[5] N. Thompson and D. J. Millard, Philos. Mag. **43**, 422 (1952).
[6] R. C. Pond and J. P. Hirth, *Solid State Physics* (Academic, New York, 1994), Vol. 47, p. 287.
[7] A. Serra, D. J. Bacon, and R. C. Pond, Acta Metall. **36**, 3183 (1988).
[8] J. P. Hirth, and J. Lothe, *Theory of Dislocations* (Krieger, New York, 1982).
[9] E. Orowan, *Dislocations in Metals*, edited by M. Cohen (American Institute of Mining and Metallurgical Engineers, New York, 1954).
[10] J. K. Lee and M. H. Yoo, Metall. Trans. A **21**, 2521 (1990).
[11] M. H. Yoo and J. K. Lee, Philos. Mag. A **63**, 987 (1991).
[12] R. A. Lebensohn and C. N. Tomé, Philos. Mag. **67**, 187 (1993).
[13] S. Mendelson, J. Appl. Phys. **41**, 1893 (1970).
[14] S. Vaidya and S. Mahajan, Acta Metall. **28**, 1123 (1980).
[15] I. J. Teutonico, Acta Metall. **11**, 1283 (1963).
[16] S. Mahajan and G. Y. Chin, Acta Metall. **21**, 173 (1973).
[17] J. A. Venables, J. Phys. Chem. Solids **25**, 693 (1964).
[18] J. B. Cohen and J. Weertman, Acta Metall. **11**, 996 (1963).
[19] S. Mahajan, G. Y. Chin, and A. W. Sleeswyk, Philos. Mag. **8**, 1467 (1963).
[20] S. Vaidya, S. Mahajan, and K. P. D. Lagerlof, Acta Metall. Mater. **41**, 2143 (1993).
[21] S. Kibey, J. B. Liu, D. D. Johnson, and H. Sehitoglu, Appl. Phys. Lett. **89**, 191911 (2006).
[22] S. Kibey, J. B. Liu, D. D. Johnson, and H. Sehitoglu, Acta Mater. **55** (20), 6843 (2007).

[23] J. Marian, W. Cai, and V. V. Bulatov, Nat. Mater. **3**, 158 (2004).
[24] R. Priestner and W. C. Leslie, Philos. Mag. **11**, 895 (1965).
[25] A. Serra, R. C. Pond, and D. J. Bacon, Acta Metall. Mater.leee **39**, 1469 (1991).
[26] A. Serra, D. J. Bacon, and R. C. Pond, Acta Mater. **47**, 1425 (1999).
[27] A. Serra and D. J. Bacon, Philos. Mag. A **63**, 1001 (1991).
[28] M. H. Yoo, J. R. Morris, K. M. Ho, and S. R. Agnew, Metall. Mater. Trans. A **33**, 813 (2002).
[29] A. Serra and D. J. Bacon, Philos. Mag. A **73**, 333 (1996).
[30] F. R. N. Nabarro, Adv. Phys. **1**, 269 (1952).
[31] J. Eshelby, Philos. Mag. **40**, 903 (1949).
[32] A. J. E. Foreman, Acta Metall. **3**, 322 (1955).
[33] S. S. Orlov and V. L. Indenbom, Sov. Phys. Crystallogr. **14**, 675 (1970).
[34] F. Kroupa, Czech. J. Phys., Sect. B **11**, 847 (1961).
[35] F. Kroupa, Acta Metall. **14**, 60 (1966).
[36] A. J. E. Foreman, Acta Metall. **3**, 322 (1955).
[37] P. G. Partridge, Metall. Rev. **12**, 168 (1967).
[38] L. J. Slutsky and C. W. Garland, Phys. Rev. **107**, 972 (1957).
[39] E. S. Fisher and C. J. Renken, J. Nucl. Mater. **4**, 311 (1961).
[40] M. I. Baskes and R. A. Johnson, Modell. Simul. Mater. Sci. Eng. **2**, 147 (1994).
[41] W. Hu, B. Zhang, B. Huang, F. Gao, and D. J. Bacon, J. Phys.: Condens. Matter **13**, 1193 (2001).
[42] A. Serra and D. J. Bacon, Mater. Sci. Forum **126-128**, 69 (1993).
[43] B. A. Bilby and A. R. Entwisle, Acta Metall. **2**, 15 (1954).
[44] S. Mahajan and G. Y. Chin, Acta Metall. **21**, 1353 (1973).
[45] M. H. Yoo, Trans. Metall. Soc. AIME **245**, 2051 (1969).
[46] L. Jiang, J. J. Jonas, R. K. Mishra, A. A. Luo, A. K. Sachdev, and S. Godet, Acta Mater. **55**, 3899 (2007).
[47] G. C. Kaschner, C. N. Tome, I. J. Beyerlein, S. C. Vogel, D. W. Brown, and R. J. McCabe, Acta Mater. **54**, 2887 (2006).
[48] L. E. Murr and S. H. Wang, Res. Mech. **4**, 237 (1982).
[49] J. C. M. Li, Trans. Metall. Soc. AIME **1**, 239 (1963).
[50] C. N. Tome and E. J. Savino, Mater. Sci. Eng. **24**, 109 (1976).
[51] D. Lin, Y. Wang, and C. C. Law, Mater. Sci. Eng., A **239-240**, 369 (1997).
[52] Y. Y. Chen, U. T. Hong, H. C. Shih, J. W. Yeh, and T. Duval, Corros. Sci. **47**, 2679 (2005).
[53] D. Mills and G. B. Craig, Trans. Metall. Soc. AIME **242**, 1881 (1968).
[54] P. Klimanek and A. Potzsch, Mater. Sci. Eng., A **324**, 145 (2002).
[55] J. Koike, Metall. Mater. Trans. A **36**, 1689 (2005).
[56] I. J. Beyerlein and C. N. Tomé, Int. J. Plast. **24** (5), 867 (2008).
[57] J. E. Bailey, J. Nucl. Mater. **7**, 300 (1962).
[58] J. I. Dickson and G. B. Craig, J. Nucl. Mater. **40**, 346 (1971).